

Synthesis And Characterization of Superparamagnetic Iron Oxide Nanoparticles For Drug Delivery Applications



**By
Hadia Riaz**

**School of Chemical and Materials Engineering
National University of Sciences and Technology
2023**

Synthesis And Characterization of Superparamagnetic Iron Oxide Nanoparticles For Drug Delivery Applications



Name: Hadia Riaz

Reg no:00000319664

**This thesis is submitted as a partial fulfillment of the requirements for
the degree of**

MS in Nanoscience and Engineering

Supervisor: Dr. Usman Liaqat

School of Chemical and Materials Engineering (SCME)

National University of Sciences and Technology (NUST)

H-12 Islamabad, Pakistan

July, 2023



THESIS ACCEPTANCE CERTIFICATE

Certified that final copy of MS thesis written by Ms **Hadia Riaz** (Registration No 00000319664), of School of Chemical & Materials Engineering (SCME) has been vetted by undersigned, found complete in all respects as per NUST Statues/Regulations, is free of plagiarism, errors, and mistakes and is accepted as partial fulfillment for award of MS degree. It is further certified that necessary amendments as pointed out by GEC members of the scholar have also been incorporated in the said thesis.

Signature: 

Name of Supervisor: Dr Usman Liaqat

Date: 04-09-23

Signature (HOD): 

Date: 5/9/23

Signature (Dean/Principal): 

Date: 6-9-23



National University of Sciences & Technology (NUST)
MASTER'S THESIS WORK
Formulation of Guidance and Examination Committee (GEC)

Form TH-1
(Must be type written)

4

Name: HADIA RIAZ NUST Reg No: 319664
 Department: Nanoscience and Engineering Specialization: Nanoscience
 Credit Hour Completed: 24 ✓ CGPA: 3.25 ✓

Course Work Completed

S/No	Code	Title	Core/Elective	CH	Grade
1	MSE-856	Nanomaterials and Processing	Core	3	B+
2	MSE-854	Characterization of Materials	Core	3	C+
3	NSE-813	Essentials of Nanoscience and Engineering	Core	3	B
4	MSE-862	Electronic and Magnetic Materials	Elective	3	A
5	NSE-812	Environmental Nanotechnology	Elective	3	B+
6	MSE-952	Materials for Biomedical Applications	Elective	3	B+
7	NSE-941	Nanocomposite Materials	Elective	3	B
8	NSE-842	Nanomaterials for Energy Applications	Elective	3	B

9 ME-898 Research Methodology
 Date: 29-05-2021

Additional 2 cr
 Student's Signature: Hadia Riaz

Exam Br
 24/6/21

Thesis Committee:

- Name: Dr. Usman Liaqat (Supervisor)
 Department: Material Engineering
- Name: Dr. Iftikhar Hussain Gul (Co-Supervisor)
 Department: Materials Engineering
- Name: Dr. Zakir Hussain
 Department: Materials Engineering
- Name: Dr. Khurram Yaqoob
 Department: Materials Engineering
- Name: _____ (External)
 Department: _____

Signature: _____
 Signature: _____
 Signature: _____
 Signature: _____
 Signature: _____

Date: 28/6/2021

Signature of Head of Department: _____

APPROVAL

Date: 20-6-2021

 Dean/Principal

Distribution

- 1x copy to Exam Branch, Main Office NUST
- 1x copy to PGP Dte, Main Office NUST
- 1x copy to Exam Branch, Respective Institute.



National University of Sciences & Technology (NUST)

FORM TH-4

MASTER'S THESIS WORK

We hereby recommend that the dissertation prepared under our supervision by
Regn No & Name: 00000319664 Hadia Riaz

Title: Synthesis and characterization of superparamagnetic iron oxide nanoparticles for drug delivery applications.

Presented on: 29 Aug 2023 at: 1400 hrs in SCME (Seminar Hall)

Be accepted in partial fulfillment of the requirements for the award of Masters of Science degree in **Nanoscience & Engineering**.

Guidance & Examination Committee Members

Name: Dr Khurram Yaqoob

Signature: 

Name: Dr Zakir Hussain

Signature: 


Name: Dr Iftikhar Hussain Gul (Co-Supervisor)

Signature: 

Supervisor's Name: Dr Usman Liaqat

Signature: 

Dated: 29.08.23


Head of Department

Date: 30/8/23


Dean/Principal

Date: 4.9.2023

School of Chemical & Materials Engineering (SCME)

Dedication

I dedicate this thesis to My Parents & My Respected Teachers without whom I would not be here. Thanks for their endless Guidance and Support

Acknowledgements

First and foremost, praises and thanks to ALLAH Almighty for the blessings he bestowed upon me, gave me strength, good health, and the ability to learn and understand to complete this research successfully. It is a genuine to express my deep and sincere gratitude to my honorable supervisor Dr. Usman Liaqat, the best mentor, for sharing his experience and wealth of knowledge through his kind supervision, valuable guidance, and timely and constructive advice which helped me extensively in accomplishing my research work. Besides my supervisor, I profusely thank my Guidance and Examination Committee (GEC) members Prof. DR. Zakir Hussain, Prof. Dr. Iftikhar Hussain Gul, Dr. Khurram, and my fellow lab mates for the guidance, timely suggestions, and effective working environment. I owe a deep sense of appreciation to the lab technicians/engineers for the characterization of samples and assistance in understanding the instrumentations. I also acknowledge the help provided by fellows from the other labs. In addition, I would like to extend my sincere thanks to my best friends for their ceaseless cooperation and support both in and outside the lab throughout my research. I would like to convey my wholehearted gratitude to all the teachers/lecturers I learned from since childhood and everyone who has directly or indirectly helped me throughout my academic journey. Last but not the least, huge thanks to my parents and husband for their unparalleled love, care, encouragement, financial and emotional support, and lots of prayers.

Hadia Riaz

Abstract

Metal–organic frameworks, generally referred to as MOFs, are a type of porous hybrid material that is made of metallic cations and organic ligands. These frameworks are being extensively examined in many possible applications. In the present investigation, magnetic metal-organic frameworks (MOFs) have been synthesized for the very first instance with the objective of facilitating drug delivery. The production of MOFs that can enclose superparamagnetic Fe_3O_4 nanoparticles has been made possible by the development of a generic coprecipitation process that can be carried out in situ in a single step. The incorporation of Fe_3O_4 nanoparticles into MOFs results in the display of numerous fascinating intrinsic features, such as a porous nature, simple functionalization, and potent superparamagnetism. In this example, Ciprofloxacin drug has been covalently linked to amino-rich magnetic MOFs. The field emission scanning electron microscopy (FESEM), the Fourier transform infrared spectroscopy (FT-IR) and X-ray diffraction (XRD) are used to analyze the magnetic MOFs that are produced as a result of this process. Drug loading was characterized by UV-VIS spectroscopy. XRD showed formation of magnetite, MOF, and functionalized magnetic MOF. SEM images confirm the formation of magnetic MOF loaded with different amount of nanoparticles. FTIR analysis confirms the loading of drug into the functionalized magnetic MOF. Increased drug loading is observed in the case of high loaded MOF having encapsulation efficiency of 87%, which also shows good drug release rate.

Table of Contents

Chapter 1:.....	1
Introduction	1
1.1 Magnetic Nanoparticles:	2
1.2 Magnetization:	4
1.2.1 Diamagnetism	5
1.2.2 Para magnetism	5
1.2.4 Superparamagnetism.....	6
1.2.5 Anti-ferromagnetism	7
1.2.6 Ferrimagnetism.....	7
1.3 Biodegradable polymer:	7
1.4 Metal organic frameworks (MOF):.....	8
1.5 Drug delivery:	9
1.6 Objectives:.....	11
Chapter 2:.....	12
Literature review.....	12
2.1 Magnetite nanoparticles:	12
2.2 Metal-Organic Frameworks (MOF):	15
2.2.1 Types of MOFs	18
2.2.2 Characteristics of MOFs:.....	18
2.3 Drug Delivery	19
Chapter 3:.....	24
Materials and Methods.....	24
3.1 Synthesis of Fe ₃ O ₄ nanoparticles:	24
3.2 Synthesis of PEG coated MNPs.....	24
3.3 Synthesis of MIL 88B:	25
3.4 Synthesis of Fe ₃ O ₄ @Fe-MOF:.....	25
3.5 Drug loading On Fe ₃ O ₄ @Fe-MOF:	25
Chapter 4:.....	26
Characterization Techniques.....	26
4.1 X-Ray Diffraction Techniques	26

4.2 Scanning electron microscopy (SEM):	27
4.3 Fourier Transform Infrared (FT-IR) Spectroscopy:	29
4.4 UV-Vis Spectroscopy:.....	30
4.4.1 Drug loading and release studies:	31
Chapter 5:.....	33
Results and discussion.....	33
5.1 X-Ray diffraction (XRD) results:	33
5.1.1 Fe ₃ O ₄ :	33
5.1.2 PEG @ Fe ₃ O ₄ :	34
5.1.3 Fe-MIL-88B-NH ₂ :	35
5.2 Fourier-Transform Infrared Spectroscopy (FTIR) Analysis:	37
5.3 Scanning Electron Microscopy:	39
5.3.1 Fe ₃ O ₄ :	39
5.3.2 Fe-MIL-88BNH ₂ :	41
5.3.3 Fe-MIL-88B-NH ₂ @ Fe ₃ O ₄ :.....	41
5.4 Drug Loading of Nanoparticles:.....	42
5.4.1 Standard Curve of Ibuprofen:	42
5.4.2 Drug Loading on Nanoparticles:	43
5.4.3 Drug Release Studies:	44
Conclusion	47
Reference:	48

List of Figures

Figure 1: Various biomedical applications of magnetic nanoparticles	3
Figure 2: Different groups of magnetic materials	5
Figure 3: Hysteresis Loop of Ferromagnetic materials.....	7
Figure 4: Experimental setup of X ray Diffraction technique	27
Figure 5: Experiential setup For Scanning electron Microscopy.....	28
Figure 6: FTIR Setup	30
Figure 7: A simplified schematic of the main components in a UV-Vis spectrophotometer	31
Figure 8: XRD Graph of Fe_3O_4	34
Figure 9: XRD graph of PEG coated Fe_3O_4	35
Figure 10: XRD graph of Fe-MIL-88B-NH ₂	36
Figure 11: XRD pattern observed for magnetic MOF loaded with 5%, 10%, 15%, and 20% nanoparticles.	37
Figure 12: FTIR pattern of Fe_3O_4 nanoparticles, PEG@ Fe_3O_4 , PEG@ Fe_3O_4 @MIL-88B and PEG@ Fe_3O_4 @MIL-88B@CIP.	39
Figure 13: SEM images of Fe_3O_4	40
Figure 14: SEM images of Fe-MIL-88B-NH ₂	41
Figure 15: SEM images of different composites (a) 5-C, (b) 10-C, (d) 15-C, (d) 20-C.	42
Figure 16: Standard curve for ciprofloxacin	43
Figure 17: percentage drug release of all composites	46

List of Tables

Table 1: Absorbance values of ciprofloxacin at various concentrations.....	43
Table 2: Encapsulation efficiency of composites.....	44
Table 3: percentage drug release data of composites.....	45

List of Abbreviations

SEM	Scanning Electron Microscope
XRD	X-ray Powder Diffraction
FTIR	Fourier-Transform Infrared Spectroscopy
UV-VIS	Ultraviolet visible spectroscopy
CIP	Ciprofloxacin
MOF	Metal organic framework
IONs	Iron oxide nanoparticles
SPIONs	Superparamagnetic Iron Oxide Nanoparticles
nm	Nanometers
MNPs	Magnetic Nanoparticles
MRI	Magnetic Resonance Imaging
EE	Encapsulation Efficiency
FDA	Food and Drug Administration

Chapter 1:

Introduction

Nanotechnology is widely recognized as a significant field of study in modern science due to its capacity to enable experts to accomplish various tasks, including researchers, scientists, and engineers. to engage in investigations and experiments at the microscopic level of cells. Nanoparticles refer to materials, either organic or inorganic, that possess dimensions within the nanometer scale, typically ranging from 1 to 100 nanometers (nm).[1], have superior properties to their bulk counterparts. Zero-dimensional nanomaterials are quantum dots, one-dimensional nanomaterials are nanoscale wires and rods, two-dimensional nanomaterials include nanofilms, nanolayers, and nanocoating such as graphene, and three-dimensional nanomaterials include nanoscale belts, sheets, disks, and films. Nanoparticles have attracted significant attention due to their exceptional optical, catalytic, electrical, and magnetic characteristics. Nanoparticles in this size range are quicker (rapid clearance and diffusion), lighter, more mobile, less expensive, and more energy efficient. This size range of nanoparticles increases adsorption, absorption, and penetration due to enhanced molecular interaction. Two primary factors account for the modification of nanoscale properties. First, the ratio of surface area to volume increases as the majority of atoms move closer to the surface, rendering them weakly bonded and more reactive. Second, there is a change in the material's electric and optical properties due to the quantum mechanical effect in which the size of the structure becomes proportional to the wavelength of the electron, resulting in quantum confinement and thus a change in the material's optical and electronic properties.

Due to these factors, enhanced properties can be observed, such as a decrease in melting point, an increase in hardness, altered optical, electrical, and magnetic properties, a self-purification process, and an increase in chemical stability. Due to the exceptional properties of these nanoparticles, there has been an unusual increase in their use in the life sciences. Nanotechnology introduces numerous applications to the biomedical field. Among these applications are drug delivery, magnetic hyperthermia, bio imaging,

sensors (bio sensors), and others. According to previous research, nanotechnology concentrates primarily on the field of biomedical science encompasses a wide range of therapeutic and diagnostic applications.

The discipline of biomedicine is increasingly inclined towards the exploitation of magnetic nanoparticles. This movement is primarily driven by the nanoparticles' biocompatibility, small sizes, ability to undergo biofunctionalization, and their responsiveness to external magnetic fields. [2-6]

1.1 Magnetic Nanoparticles:

Nanoparticles satisfy all requirements for managing newly emergent maladies over the past decade. As depicted in Figure, this has led to the widespread study, investigation, and application of biomedical applications involving magnetic materials.

Due to their exceptional properties, such as chemical stability, biocompatibility, high saturation magnetization, the ability to have interactive functions at the surface, less toxicity, and the ability to perform work at the molecular and cellular level, MNPs are gaining interest for their applications in imaging, hyperthermia, drug delivery systems, and combinational approaches for biomedical. To boost their efficacy, magnetic nanoparticles (MNPs) are commonly coupled with various materials to improve biocompatibility. These materials serve several purposes, such as carrying therapeutic payloads, encapsulating imaging agents, and providing functional groups for conjugating biomolecules. This approach is widely employed in biomedical applications. [7, 8]



Figure 1: Various biomedical applications of magnetic nanoparticles

The composition of magnetic nanoparticles (MNPs) primarily consists of nickel, cobalt, iron, or their respective alloys and oxides. Considerable attention has been directed into the deliberate fabrication of these compounds. The majority of magnetic nanoparticles (MNPs) utilized in biomedical applications consist of iron oxides, specifically Fe_2O_3 and Fe_3O_4 , as well as complex compounds of gadolinium due to their ability to decompose and be eliminated from the body of living organisms used for oxygen transport and metabolic mechanism. Iron oxide nanoparticles exhibit remarkable properties, even in the absence of an external magnetic field exhibit dispersive properties. In the presence of a magnetic field, these particles exhibit a propensity to amass at the designated location, the factor that is of utmost importance for biomedical applications. Doped IONPs such as MnFe_2O_4 and CoFe_2O_4 and metal alloy nanoparticles (e.g., FeCo and FePt) are also accessible; however, their toxic potential and rapid oxidation limit their use in biomedical applications. For biomedical applications, magnetic nanoparticles must possess the same physical and chemical properties in order to regulate bio dispersion,

contrast effect, and bioelimination. These particles would possess a greater magnetic moment, the capacity to be altered by binding to bioanalytes, and resistance to various physiological states.

Magnetite is the most favorable and prospective material for biomedical applications among magnetic nanoparticles due to its less toxic behavior, biocompatibility, magnetic properties, and approval by the Food and Drug Administration (FDA) of the United States. Utilization of magnetic nanoparticles in the morphological analysis of animal internal organs demonstrated their low toxicity.

1.2 Magnetization:

The size, charge, magnetization, surface chemistry, and morphology of MNP have a significant impact on their biodistribution and bioavailability in biological environments. A significant amount of research is being conducted on the magnetic field strength used in conjunction with nanoparticles to direct the nanoparticles to the target area and regulate their residence duration; the nanoparticles reside in the target area.

The magnetic nature of the particles is determined by the whirling and orbital motion of electrons and their interactions with one another, which generate attractive and repulsive forces. The degree of magnetization that occurs in the body when a magnetic field is applied is known as magnetic susceptibility. Coercivity is the magnetic field intensity required to reduce magnetism to zero after it has attained its maximum level, whereas remanence is the capacity of a material to retain magnetization after magnetizing force has been removed.

Several types of magnetic elements are distinguished by their magnetic susceptibility and magnetic moment orientation. Magnetism is divided into five categories based on the material's response to an externally applied magnetic field, as shown in Figure.

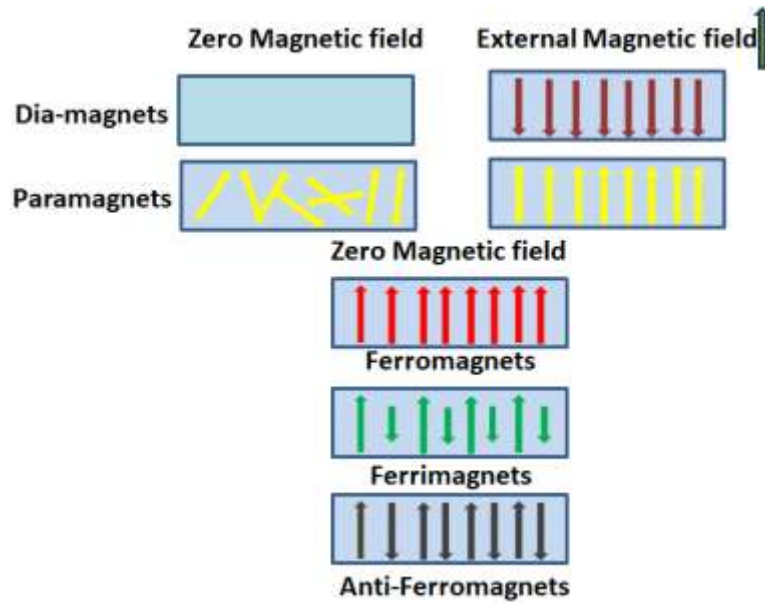


Figure 2: Different groups of magnetic materials

1.2.1 Diamagnetism

Materials exhibiting diamagnetism have zero magnetic moments because their shell orbitals are filled and there are no unpaired electrons. It is temperature and magnetic field independent. These materials exhibit a phenomenon known as diamagnetism, wherein they counteract an externally imposed magnetic field by orienting their magnetic moments in the opposite direction of the field. Consequently, these materials possess a negative magnetic susceptibility.

1.2.2 Para magnetism

Materials exhibiting diamagnetism have zero magnetic moments because their shell orbitals are filled and there are no unpaired electrons. It is temperature and magnetic field independent. These materials exhibit a phenomenon known as diamagnetism, wherein they counteract an externally imposed magnetic field by orienting their magnetic moments in the opposite direction of the field. Consequently, these materials possess a negative magnetic susceptibility.

1.2.3 Ferromagnetism

In the absence of a magnetic field, the parallel alignment of magnetic moments induces spontaneous magnetization in ferromagnetic materials. Electronic exchange forces account for parallel and antiparallel alignments. The magnetization of a ferromagnetic material exposed to an external magnetic field does not revert to a minimum when the magnetic field is shut off. When the magnetic field is applied in the opposite direction, there will be no magnetization. This inability to retrace the magnetization curve is referred to as hysteresis.

1.2.4 Superparamagnetism

In larger particles, the alignments of aligned spin magnetic moments are partitioned into domains that are separated by domain walls. Due to the dearth of domain barriers, the number of domains in a particle decreases as its size decreases, eventually dropping to a single domain, which is not energetically favorable. When the magnetic moments align in the preferable orientation, magnetic saturation of the particle is facilitated. As shown in Figure, particles with a diameter smaller than the critical diameter are superparamagnetic, exhibiting no hysteresis, zero coercivity, and zero remanence. Due to thermal effects, the magnetic moment of a material is imperfectly aligned in the direction of the applied field; however, this imperfect alignment is sufficient to demagnetize a saturated assembly of particles upon removal of the magnetic field.

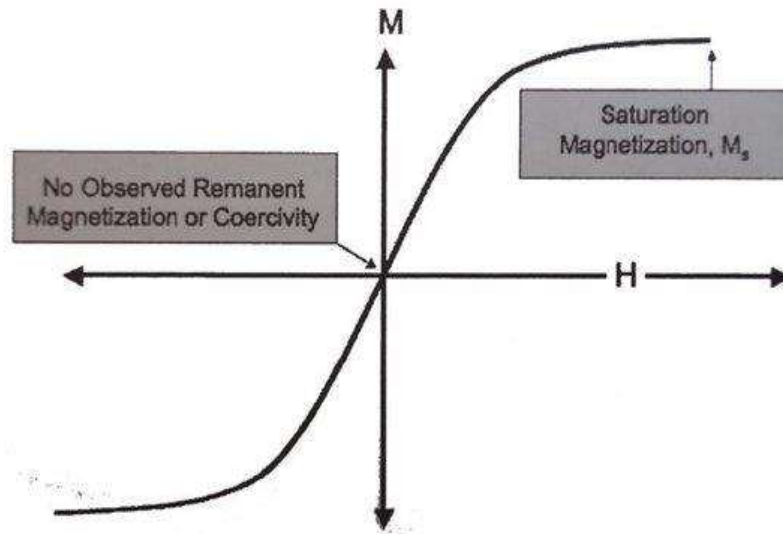


Figure 3: Hysteresis Loop of Ferromagnetic materials

1.2.5 Anti-ferromagnetism

In the absence of a magnetic field, these materials have two sublattices with magnetic moments in opposite directions that cancel out to produce zero net moment.

1.2.6 Ferrimagnetism

Due to the crystal structure consisting of two sublattices separated by oxygen ions, ferrimagnetism is prevalent in ionic compounds such as oxides. They behave similarly to ferromagnetic materials, but their magnetic ordering is quite distinct. It can be conceptualized as "imperfect antiferromagnetism" with an antiparallel arrangement of magnetic moments due to super exchange or indirect interaction mediated by oxygen ions, which do not cancel each other out as they do in antiferromagnetic materials.

1.3 Biodegradable polymer:

The surface of a material is responsible for a variety of properties, including adhesion, wettability, dissolution, and degradation, and also serves as a barrier and point of contact between the material and its external environment. Polymers are widely employed as

surface coatings in colloidal systems and the pharmaceutical industry [9]. The durability of a polymer is contingent upon its chemical and physical characteristics, alongside the magnitude and classifications of environmental degradation factors. Utilizing non-toxic, biocompatible, biodegradable, and stimuli-responsive (pH, temperature, magnetic field) polymers, magnetic polymer colloids for biomedical applications form stable aqueous dispersions at physiological pH 7.4. There are two categories of biodegradable polymers, natural and synthetic [10], consisting of ester, amide, and ether groups with distinct properties, resulting in Figure 1-10's custom-tailored materials for various applications. Both synthetic and natural biodegradable polymers are utilized in biomedical applications, but synthetic polymers offer more benefits than natural polymers[11]. Natural polymers are biocompatible and biodegradable, but their processing structure is complex, and they cannot be replicated. However, synthetic polymers are simple to produce, and their physical and chemical properties can be tailored to specific applications.

Biodegradation of the polymer into smaller non-toxic fragments is dependent on the polymer's structure and surrounding environment and is typically characterized by a decrease in molecular weight, mass, or stiffness over time. Biodegradation can range from surface erosion (only the surface of the polymer is eroded, layer by layer) to bulk erosion (the entire polymer, including the interior, is eroded).

Hydrolysis is the primary mechanism of degradation for synthetic polymers, in which water permeates the amorphous region of the polymer chain and indiscriminately fractures chemical bonds. Numerous natural and synthetic biodegradable polymers are utilized for nanoparticle surface functionalization.

1.4 Metal organic frameworks (MOF):

Metal-organic frameworks, also known as MOFs, are composite materials that exhibit a crystalline structure. The materials mentioned above consist of metallic ions or groups that serve as the central coordination center, accompanied by organic linkers that possess diverse binding sites. Organic ligands play a crucial role in facilitating the interconnection of metallic sites within the framework structure. Metal-organic frameworks (MOFs) are a class of crystalline materials that consist of metal ions or

clusters coordinated with organic ligands exhibit remarkably vast internal surface areas characterized by consistent porosity, reaching up to an impressive 6,500 square meters. These materials demonstrate notable pore dimensions, with a maximum capacity of 2 cm³/g. and possess diverse characteristics such as structure, pore diameter, and the aggregate volume of all pores. The aforementioned characteristics can be conveniently modulated through the manipulation of the constituent molecular entities. Furthermore, the surfaces of these objects can be easily altered with precise functionalities through the implementation of relatively mild conditions.

Hence, these frameworks (MOFs) have been suggested as highly potential substances for a diverse range of uses, encompassing adhesion, segregation, and storing gases.

Metal-organic frameworks (MOFs), consisting of biodegradable ions of metal and organic ligands, are being extensively studied in the realm of potential biomedical applications. Metal-organic frameworks (MOFs) exhibit exceptional suitability as carriers for drug delivery due to their remarkable ability to efficiently trap drugs within their expansive pore structure. Moreover, these MOFs possess the unique capability to precisely modulate the release of drugs by finely tuning the dimensions of their pores. Hence, Metal-Organic Frameworks (MOFs) have been extensively examined to showcase their efficacy in in vivo environments. [12]

1.5 Drug delivery:

The use of functional nanomaterials, to design hybrid nano systems that contain magnetic nanoparticles especially IONPs and stimuli responsive biodegradable polymers for controlled release of drugs under the influence of the external magnetic field, is attracting a great deal of attention because of their inherent simplicity, straightforward preparation methods, and the capacity to customize their properties to suit particular biological purposes, such as cancer therapy and the tRNA gene. For targeted drug delivery utilizing an in the presence of an external magnetic field, these nanoparticles exhibit enhanced magnetic properties to function at the cellular and molecular level of biological interactions in conjunction with drug loading capability has been intensively studied [13]. A magnetic drug delivery system typically comprises a magnetic core coated with stimuli-responsive polymers, silica, or other organic materials that can be

functionalized to achieve improved physical and chemical properties, such as good dispersion, colloidal stability against oxidation, and an appreciable amount of drug can be loaded (attached or encapsulated) within the polymer shell.[14]

The utilization of an arrangement of nanoparticles that are magnetic as a mechanism for drug delivery exhibits the ability to effectively transport the drug to the designated location, precisely at the appropriate time and concentration. Furthermore, this approach serves to safeguard non-malignant tissues in other areas of the body from potential harm.[15]

In vivo monitoring of drug distribution following administration to a specific target is made possible by magnetic nanoparticles. Using an external field, however, magnetic drug delivery methods not only offer the capacity to target medication delivery after administration, but also make it possible to monitor the drug's distribution. This system minimizes severe adverse effects by decreasing drug concentration at nontarget sites.[13, 16]

In addition, the favorable biocompatibility, biodegradability, outstanding loading capacity, and ease of surface functionalization of MNPs contribute significantly to their efficacy as drug carriers for targeted, controlled release [17]. The purpose of combining temperature- and pH-sensitive smart polymers with magnetic nanoparticles is to control the release of a substance in response to a stimulus (e.g., a magnetic field, a change in pH or temperature)[18]. In stimuli-responsive magnetic systems, the amount of the drug that is liberated at the tumor premises is determined by degradation or dissolution of the carrier particle triggered by heat or pH. As they are FDA-approved and biodegradable, poly (lactic acid-co-glycolic acid) (PLGA), poly(-caprolactone) (PCL), and their copolymers are widely used in intelligent drug delivery systems [19]. By virtue of their large surface-to-volume ratio, magnetic nanoparticles can adsorb hydrophilic/hydrophobic medications and be transported to the desired site via an external magnetic field. [20] Additionally, magnetic nanoparticles can be used to initiate controlled drug release via heat.

Numerous medicinal products, including ciprofloxacin (CIP), paclitaxel, methotrexate (MTX), curcumin and epirubicin, temozolomide (TMZ) and 5-fluorouracil, are used in

conjunction with magnetic nanoparticles. Recent research has also evaluated a novel method for the sequential release of two medicines by incorporating more than one drug into nanoparticles. The purpose of controlled drug release is to maintain an effective drug concentration at the target site with minimal toxicity.

1.6 Objectives:

This thesis has following objectives:

- Synthesis and characterization of superparamagnetic iron oxide nanoparticles via Coprecipitation route.
- The present study focuses on the synthesis and subsequent characterization of amine modified Fe-MOF.
- Synthesis and characterization of amine functionalized magnetic MOF with different loading amount of nanoparticles.
- • Assessment of drug encapsulation and drug release characteristics of amine functionalized magnetic MOF (5, 10, 15, 20% loading of magnetic particles)

Chapter 2:

Literature review

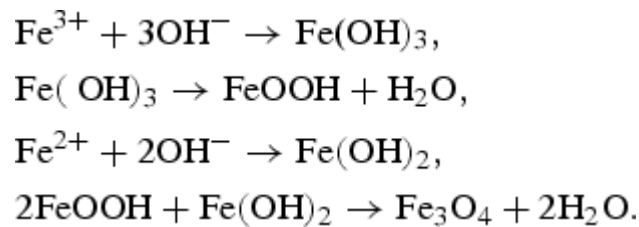
Because of the vast possibilities offered by functional magnetic nanoparticles (MNP), the design and controlled production of these particles have recently been the subject of research and exploration. Because of the mechanical and electrical properties, they possess, these materials are easily identifiable, which are determined not only by the size but also the configuration and the method used to create them. As a result, even the most basic plans to construct individualized nanoparticles in a consistent and unavoidable manner are required in order to satisfy the growing demand for producing these materials through the application of nanotechnology. Altering the configuration of the nanomaterials and fabricating them with responsive constituents were both necessary steps in order to obtain the outcomes that were needed from the nanomaterials. Alternatively, it was necessary to engross these materials within a matrix structure in order to generate a mixture of organic and inorganic nanomaterials in which the properties of the nanomaterial and the matrix would support each other.

2.1 Magnetite nanoparticles:

Magnetite nanoparticles stand out among the many phases of iron oxide nanoparticles (IONPs) Owing to the extensive range of their prospective applications within the realm of biomedicine. Consequently, magnetite nanoparticles are of exceptional significance. Magnetite is a versatile material because of its half ferromagnetism, high saturation magnetization, wide specific area, and loading capacity. Furthermore, compared to other magnetic nanoparticles, magnetite is more biocompatible.[21]

Magnetite has an inverted spinel configuration, the standard formula $A(B)_2O_4$, an FCC crystal lattice, and one unit cell comprises 8 formula units. It also has alternating tetrahedral (8) and octahedral (16) sites in its structure. In magnetite, the letters A and B stand for the cations Fe^{+2} and Fe^{+3} , respectively, and they occupy certain sites inside the crystal, whereas the anions of oxygen O^{-2} are found in the FCC places. Ferrous ions fill up half of the octahedral sites, while ferric ions are equally distributed across the octahedral sites and the tetrahedral sites.[22]

There are several methods available to us for the production of magnetic nanoparticles. Some of these methods include chemical coprecipitation, the thermal breakdown of organometallic precursors, and microemulsion approach. The alkalization of ferrous and ferric ions is a time-honored method known as co-precipitation. This method is utilized during the process of synthesizing magnetite nanoparticles. The ease with which it can be produced on a large scale and the pioneering work that was done by Massart, the process of co-precipitation has seen widespread usage in the nanoparticle's synthesis. Synthesis of nanoparticles over a wide size spectrum may be accomplished using this technology in the most expedient and cost-effective way possible. Co-precipitation has been widely described as a method for the production of magnetite nanoparticles [23-25]. This method affects the size, purity, morphology, and characteristics of the magnetite is contingent upon various factors, including pH levels, temperature, the molecular weight ratio of iron salts, and the quantity of alkaline medium. Prior to the procedure of precipitation in basic media, both ferrous and ferric salts are solvated in water. The following reaction is the typical one that takes place during the coprecipitation method, which is used to create Fe_3O_4 nanoparticles:



When the diameter of magnetite nanoparticles is reduced to less than 20 nanometers, each particle becomes a single domain and demonstrates behavior characteristic of superparamagnetic materials. Because it possesses a greater number of favorable properties, superparamagnetic magnetite is more suited for usage in biological applications. Because of the increase in the spin disorder layer, dipolar interaction, and irregular shape of magnetite nanoparticles, saturation magnetization decreases when a particle's size decreases. This is due to the fact that magnetite nanoparticles are smaller.[26]

Over the course of the past two decades, a seemingly endless amount of research has been conducted in an effort to examine and enhance various methods of manipulating

the IONP's physical and chemical characteristics. The production of discrete and individual magnetic nanoparticles is an absolute necessity in order to reap the benefits of both fundamental and medicinal research. There is a wide variety of both physical and chemical approaches that may be taken in order to build nanoparticles in such a manner that they're stabilized with biocompatible materials on the surface, making them suitable for medicinal applications. [27]. Although it is difficult to control the form and size of these particles, a significant amount of time and effort has been invested in the design, development, and refinement of a process that produces very pure nanomaterials and enables the mass manufacturing of these materials [28]. As a means of mitigating the consequences of these unwanted side effects, a wide variety of chemical procedures, the specifics of which are determined by the colloidal chemistry of the nanoparticles in solution-phase, have been investigated.

The co-precipitation method is the most straightforward approach of producing ferrite nanoparticles from ferrous or ferric salts such as chlorides, perchlorates, nitrates, sulfates, and so on. It is also the most effective. Utilizing precursors and salt in appropriate proportions is the key to obtaining spherical nanoparticles with a restricted dispersion using this process [29, 30]. The polyol process is another approach that uses polyols like ethylene glycol, which can regulate the formation of nanoparticles and limit their accumulation. Polyol process uses polyols. This approach is particularly helpful for generating dispersed magnetite nanoparticles with magnetic characteristics that may be tuned to a desired level [31, 32]. The thermal breakdown of organometallic compounds results in the production of monodispersed nanocrystals in a single reaction that may be carried out on a large-scale using reactants that are inexpensive. This approach has already been utilized to successfully manufacture a variety of nanoparticles, including magnetite, wustite, and maghemite [33-35]. The co-precipitation technique of w/o emulsions in the liquid phase is utilized in the production of microemulsions. This approach allows for the regulation of the particle size as well as the distribution of the particle in the needed proportions. It has successfully synthesized a wide range of ferrites, including zinc, nickel, bismuth, and magnetite ferrite [36-38].

Hydrothermal synthesis, which requires higher temperatures and higher vapor pressures, is a very effective method for regulating the form and size of nanocrystals [39, 40]. The process of aerosol pyrolysis involves a series of reactors operating at varying temperatures. In this technique, the aerosol droplets go through the following processes in the reactors: the evaporation of the solvent, the condensation of the solute inside the droplet, the drying process, and finally the thermolysis of the precipitated particle. This approach is helpful for estimating the sizes of particles as well as their shapes and the components that make them up. This method may also be utilized in the synthesis of maghemite spheres with hollow interiors [41]. The development of mechanical means is accomplished by the process of high-energy ball milling, which is supported by the operational stimulation of chemical processes connected to the generation of oxides. Ceramic nanoparticles may be synthesized by the use of the sol-gel technique, with metallic alkoxides serving as the precursor material. The use of this procedure results in the formation of a broad variety of compounds, some of which are ellipsoidal single-crystalline nanoparticles and others which are polycrystalline spherical nanoparticles of hematite. It is possible to acquire magnetite and maghemite nanoparticles that are able to keep their shape by employing the appropriate deoxidation-reduction reaction [42, 43]. Additionally, core-shell nanoparticles may be synthesized by the use of any vacuum technique, such as sputtering.

After acquiring these ferromagnetic nanomaterials, it is very necessary to do particle characterization in order to ascertain their size, shape, surface morphology, magnetic characteristics, and thermal properties. In order to characterize nanoparticles, a number of methods have been developed; however, none of these methods can give comprehensive information on the materials that have been investigated. Because of this, it is necessary to classify each sample using a variety of methods in order to gain an understanding of its size, structure, morphology, and catalytic characteristics.[44]

2.2 Metal-Organic Frameworks (MOF):

In 1965, Tomic published the first article on permeable substances and MOFs, that have garnered the interest of scientific researchers. The significance of the compound is decided not only by how they are utilized in regular life but also by how they will

influence the progression of human technology in the future. Porous MOFs are inorganic-organic hybrid components that are formed of metal-oxo clusters that are bonded together by organic ligands. Metal-organic frameworks (MOFs) consist of cores that have a composite composition comprising both organic and metallic components. In the context of MOF structures, the prevailing hypothesis suggests that the organic connections function as organic Secondary Building Units (SBUs) which serve as structural supports, while the metal centers are seen as inorganic Secondary Building Units that serve as "joints." The composition of MOF consists of three primary constituents: the framework structure, inorganic metal centers, and organic ligands. In comparison to zeolites, the organic and inorganic structures of MOFs, if they were built using an extended zeolite topology, would have a greater porosity and bigger pores. The enormous pore size can be attributed in part to the expanded size of inorganic SBUs as well as the network dimensions generated by the presence of massive metal clusters. In addition, a larger porosity and longer organic ligands are beneficial to huge pore diameter, this finally leads to an extended linkage between inorganic secondary building units (SBUs).

Metal-organic frameworks (MOFs) are constructed by employing diverse metallic centers and ligands, so imparting them with the advantageous ability to modulate their physical and chemical characteristics while maintaining stability [45-47]. Metal-organic frameworks (MOFs) are well recognized as a highly effective medium for the immobilization of molecular catalysts over substrates (conductive) because they have the specific surface area and maximum pore volume. Moreover, it is possible to customize these materials in order to exhibit a heightened selectivity towards a certain chemical process. Based on theoretical calculations, it may be inferred that [48, 49] the optical band gap of MOF semiconductors can be tuned between 1.0 and 5.5 eV. Metal clusters or ions, as well as rigid organic molecules bound together via coordinative bonds, perform self-assembly polymerization, that give rise to quite crystal-like constituents that are extensively extended to 3D structures. The emergence of MOF is commonly thought of as a way to mimic inorganic constituents (i.e., zeolites). The aforementioned statement serves as a broad representation of the actual result seen in the development and production of hybrids featuring consistent

microporosity [50-53]. Regarding Metal-Organic Frameworks (MOFs), the functionalization, shape, and size of pores in zeolites cannot be precisely controlled, which is contrary. The ideal/best constituents are those materials/compounds that are simple to make, have consistency, and are easy to apply. These needs can theoretically be straightforwardly answered by MOFs: The fundamental principles underlying synthetic design are inherently simple and rely solely on a systematic and precise choice of metal centers and ligands. Under specific synthetic parameters, it is possible for the molecules to undergo self-assembly and form a solid structure. The endless world of hybrid organic-inorganic combinations can be ensured by the great diversity of such simple components. However, literature review revealed the existence of some regular structural motifs in MOF synthesis, which might be used to determine their structures [54-56]

In general, organic compounds exhibit the presence of one or more nitrogen or oxygen donor atoms within their molecular framework. These molecular entities facilitate the process of intercommunication among spatially separated metal ions. Polyamines derived from benzene, oxalic acid, and imidazole, carboxylates, cyano- and pyridyl-groups, phosphonates, and crown ethers are among the prevailing organic compounds encountered in natural environments. These compounds often serve as ligands, forming coordination complexes with various metal ions. This method of molecular manipulation has been employed by scientists to predict network topologies, encompassing characteristics such as shape, size, and dimensionality control. Additionally, it has been utilized to evaluate the challenge of chemical modification of MOFs. The inclusion of functionality into linkages and the incorporation of certain reactive groups are utilized as strategies to increase the qualities of a substance, hence enabling the achievement of a desired attribute in all regions. The term "chiral" refers to a molecular entity or compound that possesses non-superimposable mirror images. A chiral center, also known as a stereogenic center, is a specific atom inside a molecule that gives rise to chirality. The chemicals that are commercially available and the linkers that may be formed from them are profoundly affected by the use of traditional in-situ preparation or organic synthesis techniques.

The connection among the dimensionality and coordination geometry of the final product is observed. Factors such as the electronic configuration, hardness or size of the metal center, and coordination modes are known to exert influence on the topology of the framework [57-60]. As an effective adsorbent for a wide range of compounds (such as antibiotics, biological compounds, gas, and toxic pollution), advanced electrochemical energy storage systems, constant and inexpensive catalysts, inexpensive and sensitive electrochemical sensors, an efficient carrier in drug delivery systems, and the best bifunctional electrocatalyst, MOFs has been extensively examined for a diverse range of practical uses.

2.2.1 Types of MOFs:

When used in conjunction with ordinal numbers, the term "MOFs," which stands for metal-organic frameworks, denotes a unique instance of a metal-organic framework. The examination of properties and structures of Metal-Organic Frameworks (MOFs) has the potential to contribute to the advancement of framework structures possessing favorable attributes, exemplified by the IRMOF-1 and IR-MOF-16 MOF families [61, 62]. Researchers in Russia [63-65] and China [66, 67] frequently use the term "metal-organic coordination polymers" with a specific chemical composition. Some MOFs are categorized based on where they were discovered, such as HKUST, UiO, LIC, MIL, etc. Another noteworthy classification of MOFs pertains to their zeolite shape. Metal ions, namely cobalt (Co), iron (Fe), zinc (Zn), and copper (Cu), are enclosed within tetrahedral structures consisting of nitrogen (N) atoms. These metal ions are further linked together by imidazole rings, which possess versatile functionalities. The fabrication of these frameworks (MOFs) can be accomplished through the implementation of the zeolite imidazolate framework (ZIF) abbreviation.. Many more designations, including MOP-1, CPL, and F-MOF-1, were used to classify synthesized research groups.

2.2.2 Characteristics of MOFs:

On the basis of a comprehension of MOFs' overall structure, some of their features can be characterized. Their incredibly high surface area, which can range between 1500 and

7000 m²/g, is perhaps their most notable characteristic. In contrast, the maximum theoretical surface area of graphene is 2,360 m²/g. This incredibly large surface area is the result of the orderly distribution of nano-scale pore cavities, the majority of which have pore sizes smaller than 1 nanometer. At this scale, the number of atoms that could fit within these pores can be measured.

MOFs are also renowned for their exceptional tunability. Due to the tunability of their characteristics (pore size and distribution, cavity size, adsorption selectivity), several different metals have been synthesized using their simple synthesis template including Zirconium, Aluminum, Zinc, Copper, and even multi-metal-based MOFs. Indeed, this is a common method for discovering novel MOFs, as evidenced by the discovery of ZIF-8a and ZIF-67, which are based on copper and cobalt, respectively, but share an organic linker. Additionally, ligand exchange or modification can be used to alter pore distributions, cavity diameters, mechanical properties, etc. These Metal-Organic Frameworks are chemically stable because their metal nodes and organic linkages form covalent and dipole interactions. It has been established that MOFs have exceptional thermal and chemical stability (though modifications are required for stability in the presence of water). Despite the fact that identifying conductive MOFs is an active area of study, especially in relation to photovoltaics and batteries, this stability is also related to its generally high resistivity and large bandgap (>5eV).

2.3 Drug Delivery:

The iron oxide nanomaterials have been approved for utilization in biological (in vivo) contexts by the Food and Drug Administration (FDA) because the mineral magnetite and maghemite occur naturally in the human body and are biocompatible. Magnetic Drug Targeting on tumor has a recovery rate of approximately 57% as the preponderance of particles are localized on the surface of the tumor. It is superior to conventional methods because only 1% of the substance can reach the target site, demonstrating exceedingly low targeting efficiency. As a result of their reduced crystallite size, superparamagnetic iron oxide nanoparticles (SPIONs) have an exceptional penetration depth of 10 to 15 centimeters. This is because they have sufficient thermal energy to oscillate in the direction of the magnetic field.

Cancer is caused by the uncontrolled division of abnormal cells, which damages organs and healthy tissues as it spreads throughout the body. It is among the primary causes of fatality throughout the globe. Traditional treatments for this disease include chemotherapy, radiation, and surgery, all of which are less effective, noncurative, time-limited, lack specificity, and have the potential to cause severe injury to healthy cells.

Doxorubicin (DOX), Docetaxel (Dtxl), Cisplatin, Bortezomib, Gemcitabine (GEM), Artemisinin, and Paclitaxel (PTX) is a frequently employed therapeutic agent in the management of cancer. DOX intercalates within the DNA of the cell and inhibits DNA replication by inhibiting topoisomerase II [68]. Dtxl inhibits cell proliferation by disrupting the dynamics of microtubules [69]. By crosslinking with DNA purine bases, cisplatin causes cellular injury. Bortezomib inhibits cell growth by inhibiting protein degradation complexes known as proteasomes. Gemcitabine inhibits DNA long chains, leading to cell death[70]. The production of free radicals by artemisinin causes cell injury and slows the division of tumor cells [71]. PTX interferes with the typical tubule dynamics necessary for cell division [72].

Due to their exceptional features, nanoscale metal-organic structures (MOFs) have been widely used as controlled routes of delivery and agents for cancer treatment. By employing Metal-Organic Frameworks (MOFs) and MOF-derived multifunctional nanomaterials, which can be conveniently synthesized at the nanoscale and possess the ability to undergo functionalization, researchers have achieved notable breakthroughs in the realm of nanomedicine. In this review, we elucidate the recent progressions in the application of nanoscale metal-organic frameworks (MOFs) as carriers for the administration of cancer theranostics drugs.

The significance of developing multifunctional metal-organic frameworks (MOFs) for delivery of drugs is emphasized by their substantial surface area and unique apertures. However, literature on this subject is notably scarce. The authors **Gao et al.** have devised an innovative drug delivery system (DDS) utilizing nanoscale metal-organic frameworks (MOFs) for the purpose of cancer diagnostics and therapy. The development of this tumor-targeting drug delivery system (DDS) utilizing metal-organic frameworks (MOFs) was achieved by employing a straightforward post-synthetic

surface modification technique. Firstly, The substance was enclosed within a magnetic mesoporous nanomaterial known as Fe-MIL-53-NH, which concurrently functioned as a contrast agent for magnetic resonance imaging. Additionally, it was observed that the Fe-MIL-53-NH₂ nanomaterial demonstrated a substantial capacity for loading 5-fluorouracil (5-FU). Subsequently, the 5-carboxyfluorescein (5-FAM) fluorescence imaging agent and the reagent designed for targeting folic acid (FA) were chemically linked to the Fe-MIL-53-NH₂ carrier loaded with 5-fluorouracil (5-FU), resulting in the development of the sophisticated drug delivery system (DDS) Fe-MIL-53-NH₂-FA-5-FAM/5-FU. Due to the implementation of a multifaceted surface-modifying technique, the DDS Fe-MIL-53-NH₂-FA-5-FAM/5-FU exhibits exceptional biocompatibility, the cellular uptake has been significantly augmented in tumor cells, a powerful inhibitory effect on cancer cell growth, outstanding fluorescence imaging abilities, and remarkable magnetic resonance imaging capability. The present investigation integrates diagnostic and therapeutic components within a unified framework employing a straightforward and effective approach, aiming to enhance the potential of Metal-Organic structures (MOFs) for the delivery of multiple modes of medication.[73]

In the past few years, there has been a significant amount of attention and resources directed into the advancement of medication delivery systems utilizing metal organic frameworks (MOFs). In order to enhance the functionality, structures often incorporate Nanomaterials, including iron oxide (Fe₃O₄), zinc oxide (ZnO), and a variety of metal oxides, as well as graphene oxide, are under consideration., and so on. In the present study, Bhattacharjee et al. investigated the Iron (III) trimesate (MIL-100(Fe)) and its blends with ZnO nanoparticles (ZnO@MIL-100(Fe)) acts as carriers for the chemotherapy drug doxorubicin hydrochloride (DOX). The blends were synthesized using two different methods: a typical HF route, in which HF acts as a crystallizing agent, and an HF-free route. DOX loading capacity and release rates substantially differ between the resultant MOF and its composites. The results of this study indicate that the loading capacity of DOX is increased by the inclusion of nanoparticles, particularly in cases where the original MOF possesses a smaller mesopore volume, such as the specimen from the HF route. Remarkably, the observed augmentation in DOX (Doxorubicin) loading exhibited a similar magnitude when comparing it to the

Fe₃O₄@MIL-100(Fe) composite, despite the substantial dissimilarities in the individual loadings of the two distinct nanoparticle entities (ZnO and Fe₃O₄). Conversely, the inclusion of zinc oxide nanoparticles results in reducing the loading capacity of DOX when the MOF possesses a higher pore volume, as shown in the sample generated by a procedure that does not involve the use of hydrofluoric acid. The binding ability of composites synthesized by the HF method is increased, leading to a slower release of DOX due to a more pronounced interaction between the drug and the composite material. [74]

In their study, **Kim et al.** proposed NH₂-MIL-88(Fe) as a promising metal-organic framework (MOF) for the purpose of ocular medicine delivery by topical administration. The confirmation of the structural composition of NH₂-MIL-88(Fe) particles, which were synthesized by a solvothermal process, was achieved through the utilization of several analytical techniques. The integration of the anti-glaucoma medication brimonidine into NH₂-MIL(Fe)-88, denoted as NH₂-MIL(Fe)/Br., led to a loading capacity of 121.3 g/mg and a prolonged release of the medication lasting for a duration of 12 hours. The NH₂-MIL-88(Fe)/Br revealed mucoadhesive characteristics and exhibited the aforementioned characteristic. a prolonged ocular retention time of up to 4 hours in the eyes of rabbits. Consequently, following the management of NH₂-MIL-88(Fe)/Br, An appreciable quantity of brimonidine was observed in lacrimal secretions for a prolonged period. As a result, there was a notable extension in the duration of drug bioavailability and activity, exceeding that of Alphagan P, a clinically approved formulation of brimonidine eye drops. Therefore, NH₂-MIL-88(Fe) is proposed as a promising carrier for the transdermal administration of ocular medication owing to its capacity to improve the bioavailability of ocular medications.[12]

Fabrication of MOFs encapsulating superparamagnetic Fe₃O₄ nanoparticles, **Samui Et. al.** devised a general one-step in situ hydrothermal route. The incorporation of Fe₃O₄ nanoparticles into MOFs exhibits a number of fascinating intrinsic properties, such as a porous nature, simple functionalization, and strong superparamagnetism. In this study, lipase derived from *Candida rugosa* (CRL) is immobilized by covalent bonding onto amino-rich magnetic metal-organic frameworks (MOFs). Next, a comparison is made

between the enzymatic activity of CRL that is immobilized and CRL that is not immobilized. The immobilized form of CRL exhibited enhanced pH tolerance and higher thermal stability compared to the free form of CRL. The primary objective of this experiment is to ascertain the values of the Michaelis-Menten kinetic constant (K_m) and maximal response velocity (V_{max}) for lipase in its free form and when immobilized. Quantification of CRL deposited on magnetic MOFs yielded a value of 280 mg per gram of support. In addition, it was observed that the immobilized CRL had the capacity to undergo recycling for a total of nine consecutive cycles. [75]

The solvothermal method was employed by **Nasarabadi et al.** to synthesize UiO-66 nano-porous materials. Subsequently, the researchers conducted antimicrobial drug encapsulation within UiO-66 nanoparticles. The following computation revealed that 84% of the detection of drug encapsulation on the UiO-66 nano-porous metal-organic structure was studied. Furthermore, an examination was conducted on the drug release characteristics of ciprofloxacin (CIP) in solutions of phosphate buffer saline, (pH: 7.4) and acetate buffer, (pH: 5.0). The results of the investigation demonstrated that 80% , 87% of the drug were discharged after a span of three days, respectively. [76]

As a carrier for ciprofloxacin (CIP), **Forouzan Et. al.** made use of $Fe_3O_4@PAA@MIL-100(Cr)$ MOF in this particular body of work. The findings of this research indicated that the antibacterial antibiotic ciprofloxacin may be successfully encapsulated in $Fe_3O_4@PAA@MIL-100(Cr)$ at a drug loading of fifty percent by weight. In addition, drug release was carried out at pH 7.4 and pH 5.5 throughout a span of three days; this resulted in approximately 80% of the medication being released at pH 7.4. In addition, the findings of the release analysis that was performed using kinetic equations were found to be adequate. By using the disk diffusion technique, the antibacterial activities of $Fe_3O_4@PAA@MIL-100(Cr)$ and $Fe_3O_4@PAA@MIL-100(Cr)@CIP$ were put to the test against *Escherichia coli* and *Staphylococcus aureus* bacteria. Both of these materials exhibited unexpectedly high levels of antibacterial activity. [77]

Chapter 3:

Materials and Methods

3.1 Synthesis of Fe₃O₄ nanoparticles:

The nanoparticles were created using the co-precipitation process, which is explained below: Dissolve 8mmol FeCl₃.6H₂O and 4mmol FeCl₂.4H₂O in 100ml deionized water in presence of air. 5mL solution of aqueous ammonium hydroxide (NH₄OH-32%) was promptly added to it. The solid particles were let to undergo sedimentation at the base of the container when the system achieved a precipitation state. Following the occurrence of precipitation, the liquid supernatant is separated by decantation. The precipitates underwent many water washes until a pH level of 7 was attained. Subsequently, the rinsed precipitates were subjected to separation and subsequently subjected to a drying process in a vacuum oven at a temperature of 60 °C for an extended period of time. Following this, the dried precipitates were further processed into a finely powdered form [271].

3.2 Synthesis of PEG coated MNPs:

The production of PEG coated magnetic nanoparticles (MNPs) involved the utilization of an in-situ coating technique. In this process, PEG 600 Da was added into the solution having iron salts prior to the addition of ammonium hydroxide solution. Following a series of three washes using deionized water, the resultant black precipitate was effectively isolated through the process of magnetic decantation and subsequently subjected to air drying at ambient room temperature.

3.3 Synthesis of MIL 88B:

Dissolve 2.16g of $\text{FeCl}_3 \cdot 6\text{H}_2\text{O}$ in mixture of 12.4ml of DMF and 7.6ml of DI water, 0.72g of NH_2BDC in 20ml of DMF. Add salt solution into the ligand and stir it for 24 hrs. to get homogeneous mixture. Centrifuge the solution at 3000rpm for 15 min. Wash 3-4 times with ethanol. Vacuum dry at 60 degrees Celsius overnight, then grind into a fine powder.

3.4 Synthesis of Fe_3O_4 @Fe-MOF:

The Fe_3O_4 @Fe-MOF samples were synthesized through the utilization of an in situ coating technique. In this process, Fe_3O_4 particles coated with PEG were incorporated into a solution containing iron salts, followed by the addition of a ligand solution. Different loading amounts of PEG-coated Fe_3O_4 were employed in the fabrication process. The loading quantities of polyethylene glycol (PEG) coated iron (III) oxide (Fe_3O_4) nanoparticles were observed to vary at different percentages, specifically 5%, 10%, 15%, and 20%, respectively. The resulting solution underwent centrifugation and subsequent desiccation following a trifold ethanol wash.

3.5 Drug loading On Fe_3O_4 @Fe-MOF:

Ciprofloxacin drug was used as sample drug to load. 100mg of Fe_3O_4 @Fe-MOF nanocomposite was added into 10ml of DOX solution (20mg/ml) for each composition and the drug was subjected to gentle mixing for a duration of 5 days in order to facilitate its loading process. Subsequently, the drug-laden specimen underwent separation via the centrifugation technique, employing a rotational speed of 4000 revolutions per minute (rpm) for a duration of 15 minutes. Perform a triple wash using methanol. The residual supernatant was subjected to analysis utilizing a UV-visible spectrophotometer to obtain

the absorption spectrum at a wavelength of 323 nanometers, with the purpose of determining the quantity of unbound drug present.

Chapter 4:

Characterization Techniques

4.1 X-Ray Diffraction Techniques:

A nondestructive method for determining the lattice spacing of crystalline materials, which can be used to evaluate elastic properties, residual stresses, and the identification of unknown materials. When x-rays with known wavelengths and angles enter a substance, they travel through atomic planes and are refracted to a diffractometer, which records the intensity. X-rays are directed at the sample from a variety of angles to activate planes at various angles, allowing for accurate identification of planes present. Powder samples' Miller indices (hkl) and atomic spacing are frequently determined by exposing them to X-rays. The intensity measurements pertain to a particular element or phase. There are many intensity peaks in the sample.

When electrons from a heated filament strike a copper target material and dislodge the inner shell electrons, X-rays are produced. These Collimated X-rays are focused onto the

sample, where they deflect back by obeying Brags' law via constructive interference and are recorded by a diffractometer, which converts these signals to counts (peaks) displayed on a computer screen.

X-Ray Diffraction is used to determine the orientation of crystalline phases. In addition, it is employed to ascertain structural characteristics such as particle size, strain, lattice parameters, atomic arrangement, phase composition, and measurement of thin films and multilayer materials.

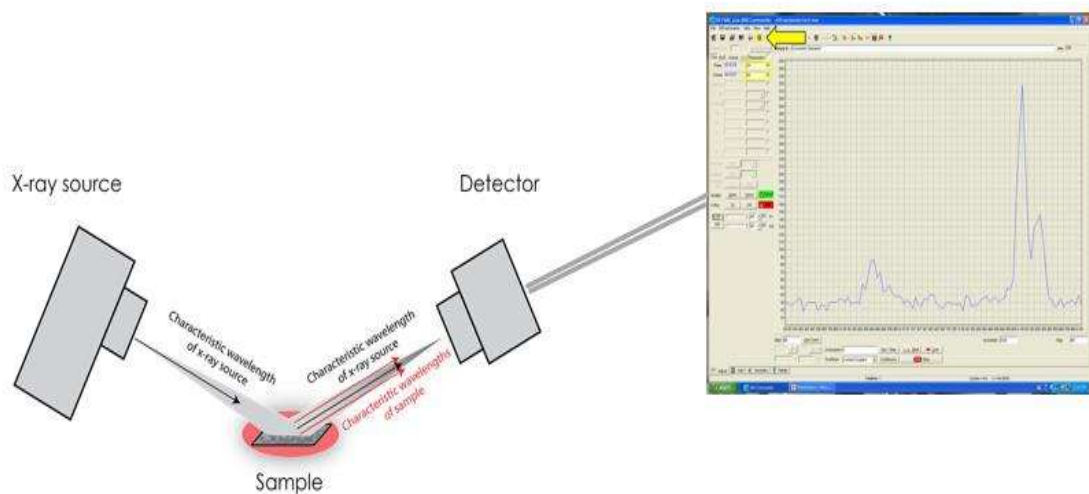


Figure 4: Experimental setup of X ray Diffraction technique

4.2 Scanning electron microscopy (SEM):

In this technique, electron beams with high energy are used to generate a variety of signals. Surface morphology, orientation, chemical composition, and crystalline structure of a material are some of the information derived from electron sample interaction. Typically, a 2-dimensional image of the surface properties of the samples is generated. Using a scanning electron microscope with a resolution of 50 to 100 nanometers and a magnification range of 20X to 30000X, an area of up to 5 microns can be imaged. Energy dispersive X-ray (EDX) can be used in scanning electron microscopy to determine chemical composition, allowing for selective analysis.

By interacting with the sample, accelerated electrons generate a variety of signals. These signals consist of secondary electrons (used to determine morphology and topography), backscattered electrons (used to demonstrate compositional contrast), photons (used for elemental analysis), visible light, and heat. SEM is regarded as a "non-destructive" technique because the production of various signals does not result in volume loss; therefore, the same sample can be tested repeatedly.

To prepare the samples for characterization of the nanoparticles, the nanoparticles were sonicated in deionized water for one to two hours. The mixture was then poured onto a glass slide and dried at 60 degrees Celsius for one hour. The glass slide was then set on a stem and gold-plated to make the sample conductive. Following this, the sample was placed in a low-vacuum chamber for SEM analysis. Images were captured with varying magnification and resolution using 20 kV of accelerating voltage.

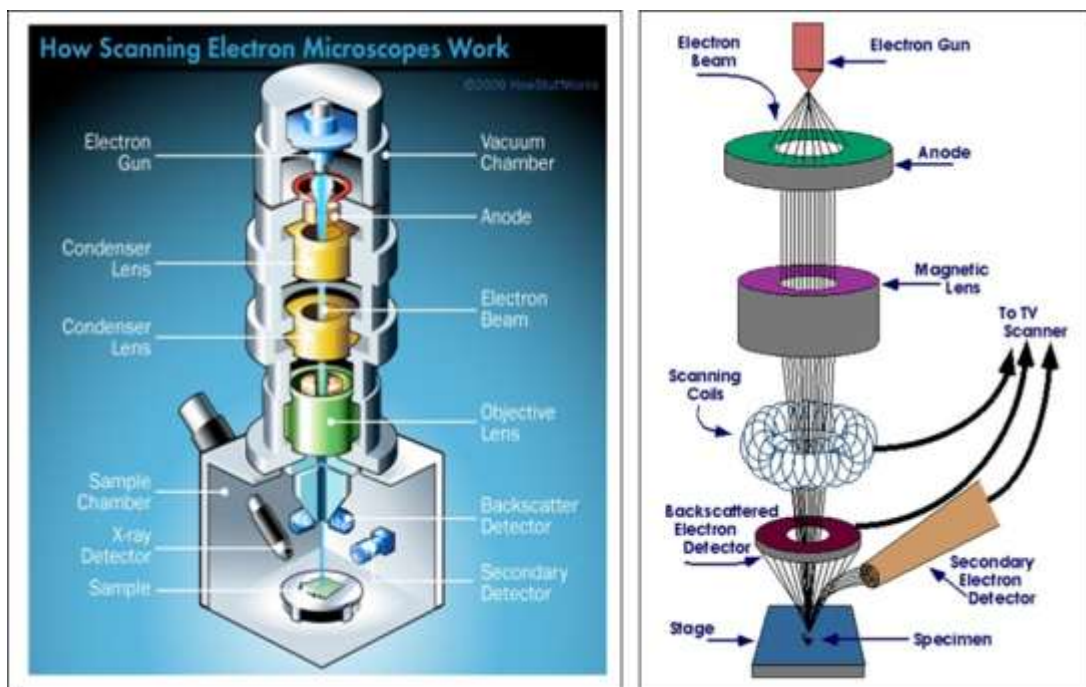


Figure 5: Experiential setup For Scanning electron Microscopy

4.3 Fourier Transform Infrared (FT-IR) Spectroscopy:

The field of infrared spectroscopy investigates the interactions between matter and infrared light. The wavelength of infrared radiation is longer than that of visible light. When these infrared wavelengths are absorbed by molecules within a material, the radiation energy absorbed is equivalent to the material's vibrational transition energy. As this vibrational energy is also associated with various rotational energies, the band shape following IR absorption is specified. These vibrational transitions are recorded as peaks and are located between 4000 and 1300 cm^{-1} . Stretching of single-bonded atoms occurs between 4000 and 2500 cm^{-1} , and if hydrogen bonding is present in this region, peak broadening will be observed. Triple-bonded atoms exhibit these frequencies between 2700 and 1800 cm^{-1} . Double-bonded atoms vary between 1950 and 1450 cm^{-1} . The frequency region below 1300 cm^{-1} is referred to as the fingerprint region because its bands contain distinct peaks that are associated with specific compounds. The operation of this spectrometer begins with the emission of infrared (IR) rays from a source, which are then directed by an interferometer consisting of movable and immovable mirrors that partially reflect and focus IR radiation on the sample, before collecting and refocusing the radiation on the detector. The obtained frequencies are then transformed by Fourier using a computer algorithm that generates a graph.

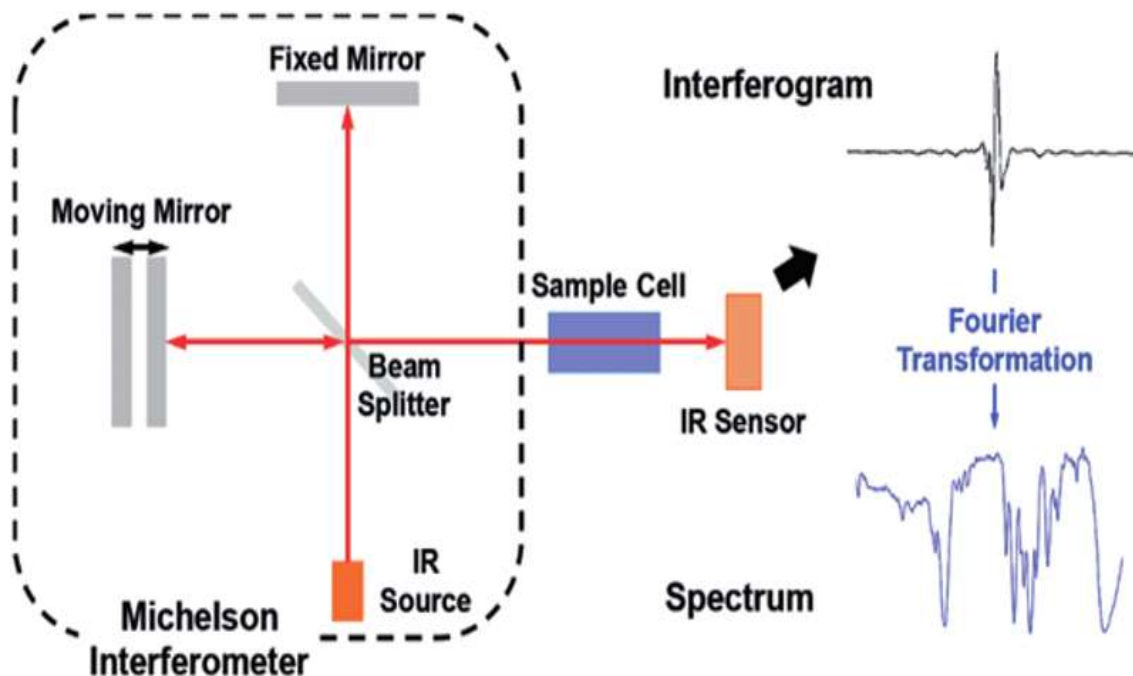


Figure 6: FTIR Setup

4.4 UV-Vis Spectroscopy:

This technique is based on the principle that the quantity of ultraviolet (UV) or visible light absorbed by a sample compared to a reference/blank sample provides information about sample specification (as specific materials absorb light at specific wavelengths) and its composition. UV light is typically used to characterize the sample because UV light has shorter wavelengths than visible light and therefore generates higher energy (frequency). A sample's maximal absorbance at a particular wavelength is used to derive information about the substance.

A high intensity light source, typically Xenon lamps, is used to generate light that is filtered by a monochromator to the desired wavelength and to enhance the signal-to-noise ratio before being transmitted through a reference sample and a sample to be

tested.

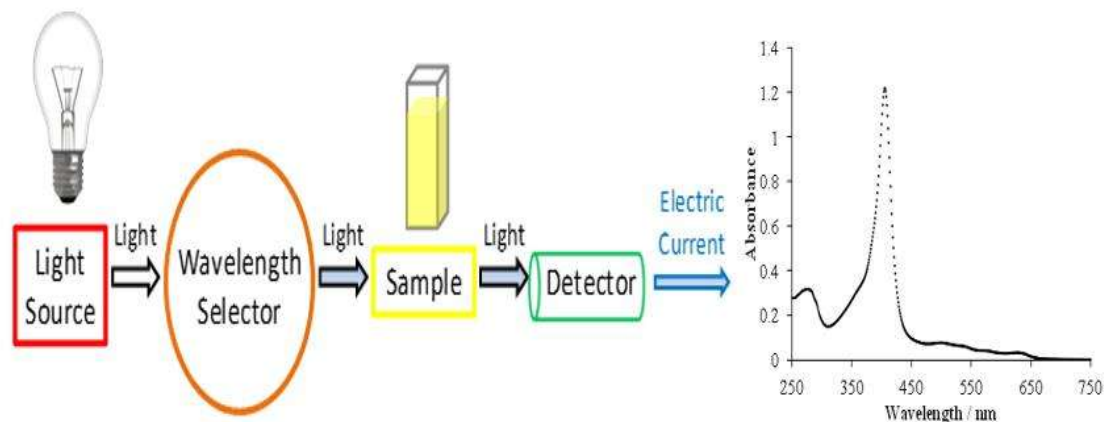


Figure 7: A simplified schematic of the main components in a UV-Vis spectrophotometer

Quartz Cuvettes are used as sampling receptacles. Both the reference and primary sample cuvettes are initially filled with the same medium. After one cycle, a blank cuvette is substituted with a sample-containing cuvette containing the same solvent used previously for characterization. A detector detects the signals and displays them on a monitor as a graph between absorbance (Y-axis) and wavelength (X-axis).

The identified absorbance value equals the intensity of light before passing through the sample (I_0) divided by the intensity after passing through the sample (I). The transmission values are derived from the inverse relationship between these two quantities and transmission values. When quantities such as molar absorptivity, path length, and absorbance values are known, the concentration of the sample in mol L⁻¹ can be calculated using Beer-Lambert's law.

$$A = \epsilon Lc = \log_{10}\left(\frac{I_0}{I}\right) = \log_{10}\left(\frac{1}{T}\right) = -\log_{10}(T)$$

To characterize the nanoparticles, all samples were dissolved in de-ionized water at a ratio of 1mg/ml solute to solvent. The sample was contained in quartz cuvettes, and a characterization range of 200-300 nanometers was applied.

4.4.1 Drug loading and release studies:

The drug loading capacity of nanocomposites was estimated using calculations utilizing UV-Vis Spectroscopy at a wavelength of 363 nm. Ciprofloxacin serves as a representative pharmaceutical compound for the purpose of loading onto these nanocomposites. In order to establish the standard curve of ciprofloxacin, several dilutions were made using deionized (DI) water as the solvent. These dilutions ranged from 0.2 mg/ml to 0.9 mg/ml of ciprofloxacin solution in DI water. A linear plot of ciprofloxacin was generated for the purpose of determining the quantity of drug loaded. To initiate the loading process of nanoparticles, a quantity of 100 mg of nanocomposite was introduced into 10 ml of deionized water for each composition. Subsequently, a quantity of 200 mg of ciprofloxacin was introduced into the solution. The medicine was loaded into each composition solution by stirring for a duration of 5 days. Subsequently, the drug-laden sample was subjected to a centrifugation procedure at a rotational speed of 4000 revolutions per minute (rpm) for a duration of 15 minutes. The quantity of unloaded medication in the leftover supernatant was assessed by analyzing its absorption spectra at a wavelength of 323 nanometers using a UV vis spectrophotometer. The determination of encapsulation efficiency was conducted using the following equation:

$$\text{Encapsulation efficiency(\%)} = \frac{\text{Initial drug weight} - \text{Free drug weight in supernatant}}{\text{Initial drug weight}}$$

The measurement of the release of the medicine was performed by sending samples loaded with the drug to analysis in a saline solution. The specimen containing the medication were distributed in phosphate buffer saline at a temperature of 37°C while being continuously stirred. At predetermined time intervals, a 5ml aliquot of the solution is extracted and replaced with an equivalent volume of new PBS solution, therefore maintaining the total volume constant. The quantification of drug release was conducted by using UV-vis spectroscopy at a wavelength of 323nm, with soaking time being the independent variable. The amount of drug released is evaluated on the basis of following equation:

$$\% \text{ Drug content} = \frac{\text{Amount of drug detected}}{\text{Theoretical amount of drug used}} * 100$$

Chapter 5:

Results and discussion

5.1 X-Ray diffraction (XRD) results:

5.1.2 Fe₃O₄:

The tiny particles underwent X-ray diffraction (XRD) examination in order to determine their structural characteristics and determine the dimensions of their crystallites. The

graph depicts the observed trends of X-ray diffraction emanating from the desiccated sample, unveiling a series of six discernible peaks. The diffractions of the [2 2 0], [3 1 1], [4 0 0], [4 2 2], [5 1 1], [4 4 0], and [533] crystalline planes are associated with distinct peaks seen at 2θ angles of 30.2° , 35.5° , 43.2° , 53.5° , 57.2° , 62.7° , and 74.4° [78-80]. The diffraction pattern examination of the sample indicated the presence of a cubic spinel structure, namely the inverse cubic spinel phase that occurs in Fe_3O_4 (magnetite, Ref-code 00-003-0863). This was supported by the observation of the greatest reflection originating from the [311] plane. The magnetite nanoparticles that were synthesized had a crystalline form that was consistent with the previously reported geometry of an inverse spinel-type oxide. This finding serves as confirmation of the nanoparticles' crystalline nature.[80]

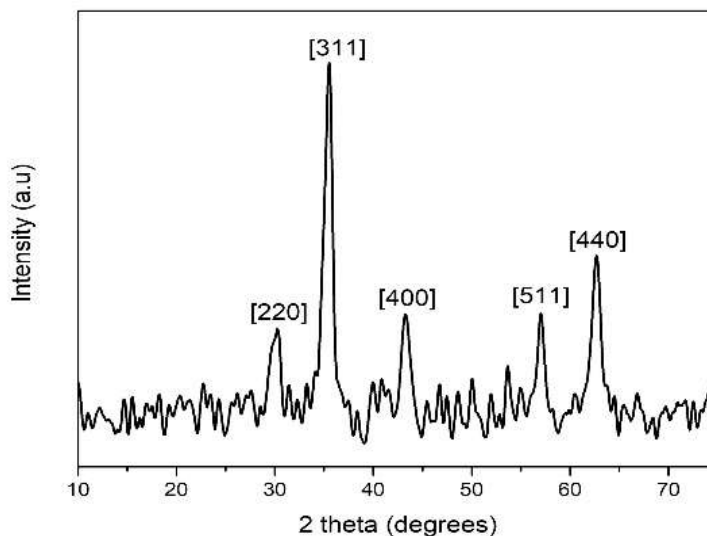


Figure 8: XRD Graph of Fe_3O_4

5.1.2 PEG @ Fe_3O_4 :

The positions and relative intensities of all diffraction peaks seen in the experiment are consistent with those recorded on the JCPDS card (19-0629) for magnetite. Specifically, the (220), (311), (400), (551), and (440) peaks were identified at about 2θ values of 30, 35, 43, 57, and 63, respectively. Nevertheless, the diffraction peaks seen in the modified

MNPs samples that have been coated with PEG exhibit a reduction in both their maximum intensity and a notable increase in their range.[79]

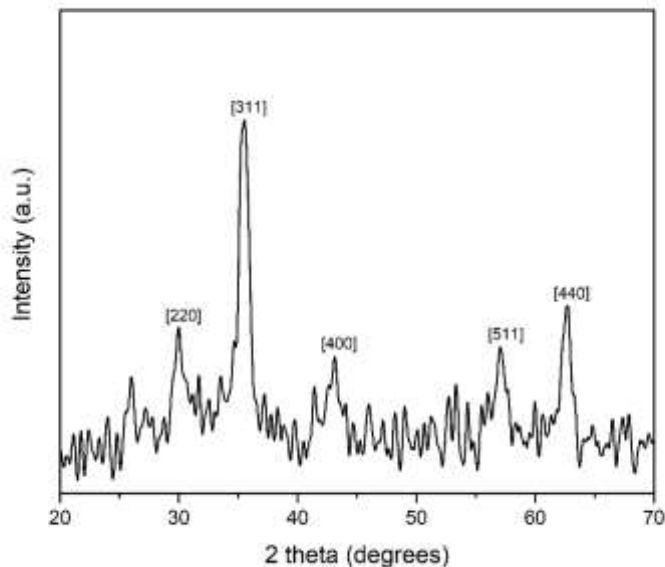


Figure 9: XRD graph of PEG coated Fe_3O_4

5.1.3 Fe-MIL-88B-NH₂:

The X-ray diffraction (XRD) pattern of Fe-MIL-88BNH₂ microcrystals reveals a prominent diffraction peak at a 2θ angle of 12.2, indicating the highest intensity of diffracted X-rays. The discrepancies found in both the intensity and the 2θ position of the reflections can be attributed to the intrinsic flexibility in structure demonstrated by MIL-88B. It is worth mentioning the movement of the skeleton, together with changes in location and variations in reflection intensity, can be attributed to the presence of visiting species (both organic and inorganic) within the pore channels, which contribute to the structural flexibility.

The extent of pore-filling and the characteristics of the visitors exert a notable influence on the magnitude of the motion. The elimination of guest molecules from the pore

channels of big MOF crystals (micro size) is often more challenging compared to tiny MOF crystals due to the presence of longer diffusion paths.[81]

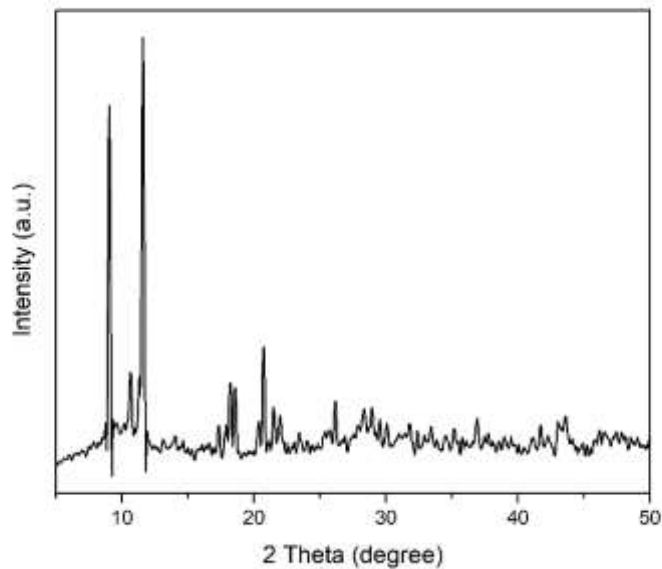


Figure 10: XRD graph of Fe-MIL-88B-NH₂

Further composition of nanocomposites PEG@ Fe₃O₄@Fe-MIL-88B-NH₂ are termed as 5-C, 10-C, 15-C, 20-C loaded with 5%, 10%, 15%, 20% nanoparticles respectively show a slight difference in the peaks recorded. The MOF suppresses peaks of nanoparticles.

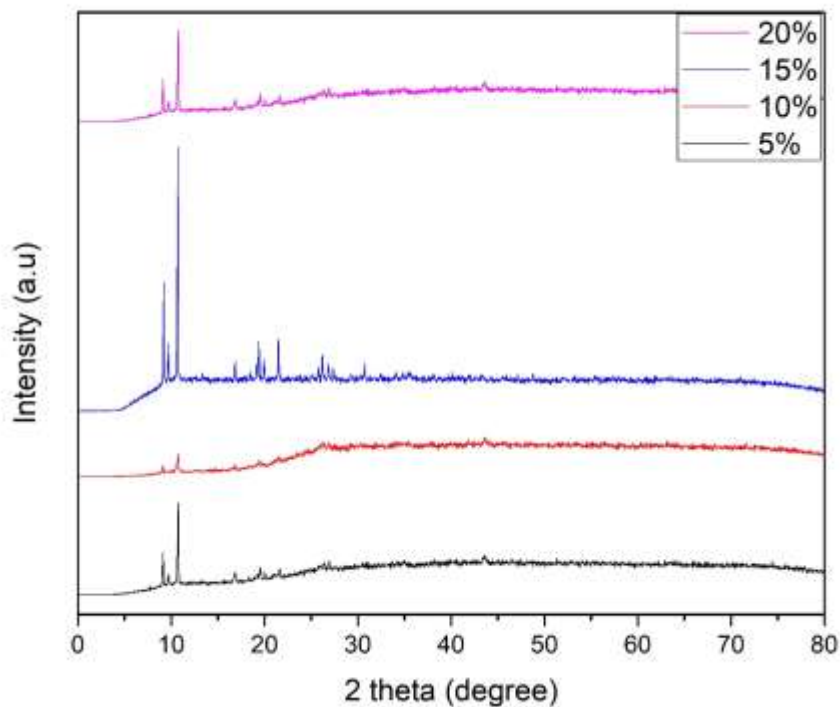


Figure 11: XRD pattern observed for magnetic MOF loaded with 5%, 10%, 15%, and 20% nanoparticles.

5.2 Fourier-Transform Infrared Spectroscopy (FTIR) Analysis:

The FTIR spectra of Fe_3O_4 nanoparticles shows multiple peaks, at $3389.34/\text{cm}$ is the O-H stretching vibration, at $1621.14/\text{cm}$ is the H-O-H bending vibration due to unabsorbed water present on the surface of nanoparticles. These two peaks correspond to the hydroxyl groups attached to the iron oxide surface by hydrogen bonds and the water molecules chemically adsorbed to the magnetic particle surfaces. The sample exhibits two intensive absorption bands at $583/\text{cm}$, which were ascribed to stretching vibrations related to the metal in the octahedral and tetrahedral sites of the oxide structure and were prominent for all spinel structures and ferrites in particular. The strong absorption peak at $583.59/\text{cm}$ was owing to magnetite nanoparticles' Fe-O stretching vibration. The peak at $441.79/\text{cm}$ is caused by the presence of Fe at the octahedral site and corresponds to the band of bulk magnetite's Fe-O. [82]

In order to conduct a more comprehensive examination of the adsorption of polyethylene glycol (PEG) onto the surface of the manufactured magnetic nanoparticles (MNPs), Fourier Transform Infrared (FTIR) analysis was carried out. The peak found at a wavenumber of 1633/cm in the PEG parameter can be ascribed to the stretching of the hydroxyl (-OH) band and the asymmetric carboxylate (COO-) stretching vibration. On the other hand, the peak at 1403/cm can be associated with the vibration of the methyl (-CH) group. The presence of these peaks, which are indicative of the -CH and -COO bonds, provides strong support for the hypothesis that the surface of the produced MNPs has undergone a coating process involving Polyethylene glycol (PEG) exhibits coordination behavior through its carbonyl group. The Fourier Transform Infrared (FTIR) spectra of magnetite nanoparticles (MNPs) coated with polyethylene glycol (PEG) revealed the absence of discernible peaks corresponding to the stretching vibrations of carbon-carbon (C-C) bonds and carbon-oxygen-carbon (C-O-C) bonds in the PEG polymer. These peaks are typically observed at wavenumbers of around 950/cm and 1080/cm, respectively. The result suggests the existence of a dipole-cation interaction among the ether group of polyethylene glycol (PEG) and the charged surface of magnetic nanoparticles (MNPs).[79]

Bands at 3490, 3370, and 1628/cm in the FTIR spectrum of NH₂-MIL-88B indicate the presence of amino groups due to symmetric stretching, asymmetric stretching, and bending vibrations, respectively. A doublet with one band at 575/cm and another at 479/cm has been attributed to the metal-organic framework's Fe-O vibration. Nonetheless, after compositing with Fe₃O₄, the adjacent bands at 3490 and 3370/cm merged with the -OH band to form a broad band at 3420/cm, whereas the other bands appeared in nearly the same positions but with varying intensities.[75]

The FT-IR spectrum of CIP-MIL-88B- Fe₃O₄ represents the molecules of CIP trapped in MIL-88B. The identification of asymmetric and symmetric properties of the carboxylate group in CIP anions in the absorption bands at 1691 and 1402/cm respectively. The modest shift of the carboxylate group in CIP from 1709/cm to 1691/cm is attributed to the interaction among CIP and UiO-66. The frequency of 1626/cm corresponds to stretching of C=O carbonyl. [76]

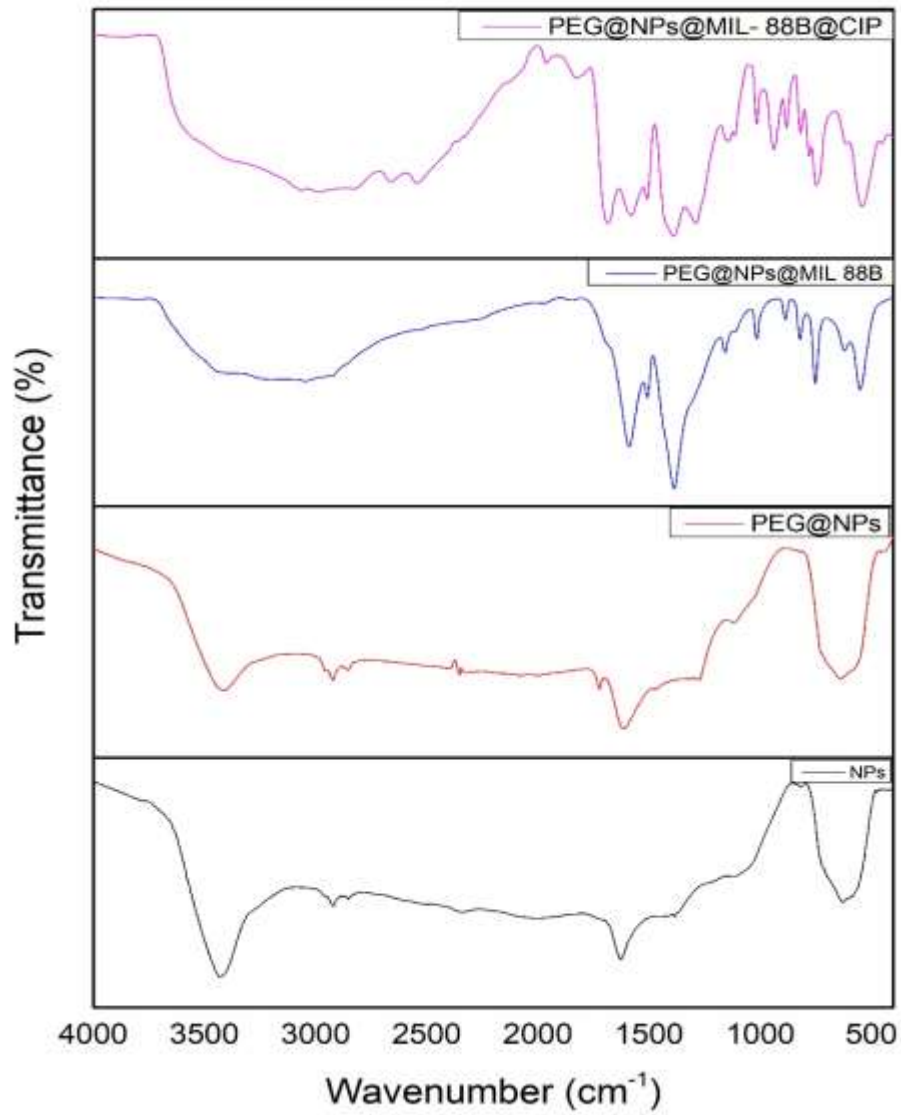


Figure 12: FTIR pattern of Fe_3O_4 nanoparticles, PEG@ Fe_3O_4 , PEG@ Fe_3O_4 @MIL-88B and PEG@ Fe_3O_4 @MIL-88B@CIP.

5.3 Scanning Electron Microscopy:

5.3.1 Fe_3O_4 :

The utilization of scanning electron microscopy (SEM) was employed to examine the dimensions and morphology of magnetite nanoparticles that had been produced through the process of co-precipitation. A little amount of the powder sample was dissolved in water, and then ultrasonication was performed on the mixture for one hour. After being dried, A single droplet of the dispersed sample was carefully deposited onto a glass slide, followed by the application of a thin layer of gold via sputtering. Pictures from a scanning electron microscope (SEM) are shown in Figure. These pictures demonstrate that magnetite particles have a roughly spherical shape, are made of nanosized particles, and are reasonably uniform. The nanoscale aggregates of numerous nanoparticles can be attributed to the dipolar and magnetic interaction among the particles, which occurs at the nanoscale. Particles were able to aggregate because they possessed a large specific surface area, which led to an elevated level of surface energy. The particles exhibit a limited size distribution, with a mean size of 22 nm with a standard deviation of 0.84 nm. The fact that the size100 predicted from the SEM picture is larger than the mean crystallite size indicates that The particles exhibit a polycrystalline structure, characterized by the presence of grain boundaries.[82]

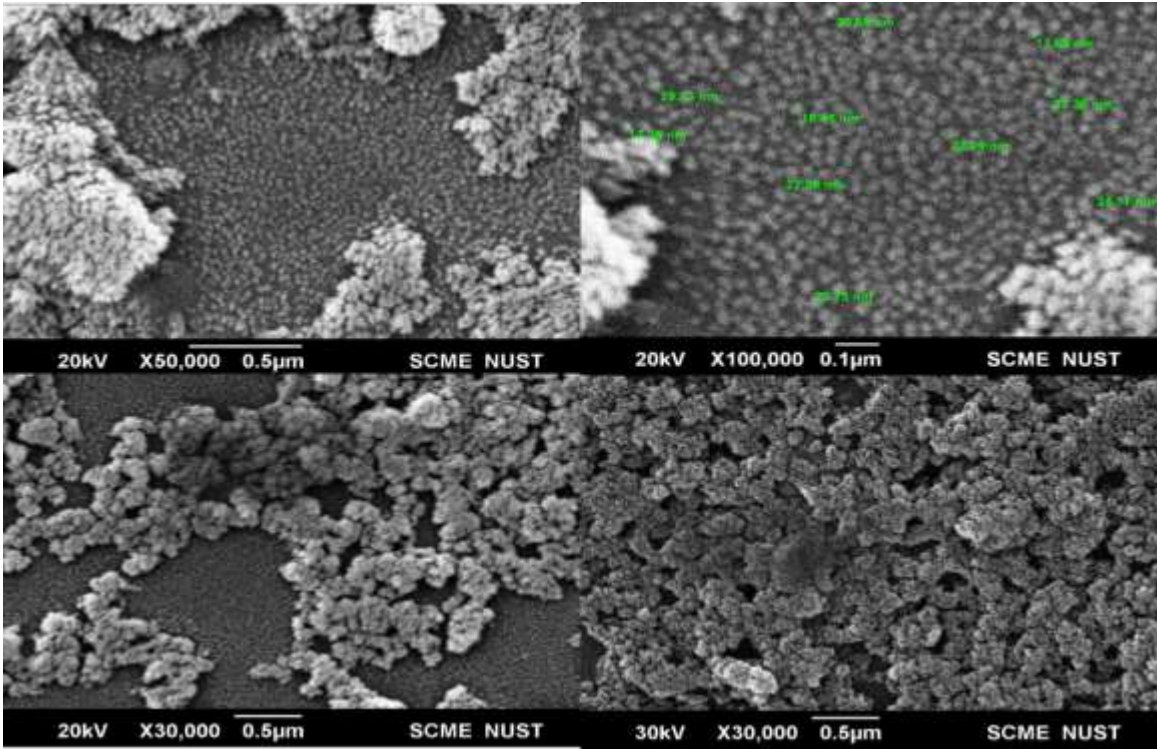


Figure 13: SEM images of Fe_3O_4

5.3.2 Fe-MIL-88BNH₂:

An aqueous reaction mixture consisting of FeCl₃·6H₂O and H₂N-BDC was used to form homogeneous Fe-MIL-88BNH₂ micro sized crystals. These crystals had the shape of a bipyramidal hexagonal prism.

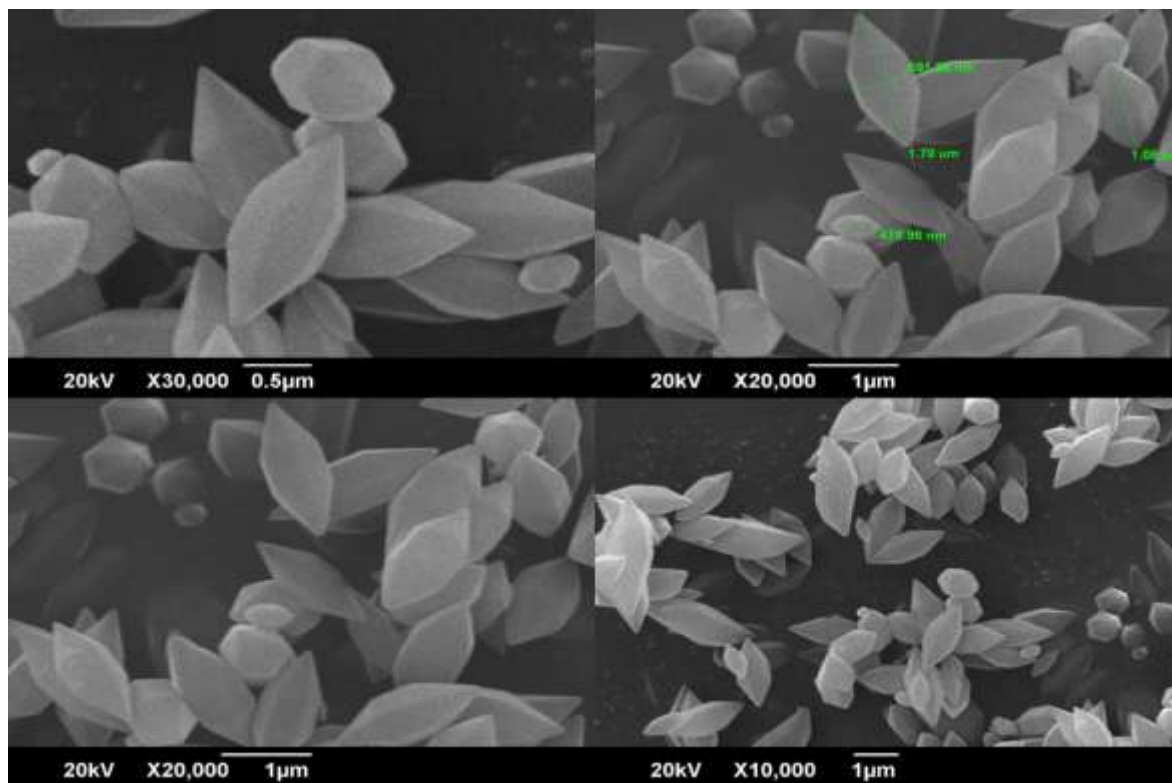


Figure 14: SEM images of Fe-MIL-88B-NH₂

5.3.3 Fe-MIL-88B-NH₂@ Fe₃O₄:

There is clear evidence that Fe₃O₄ nanoparticles have been deposited onto the MOF surface, as seen by the following pictures. The synthesis of NH₂-MIL-88B/ Fe₃O₄ takes place under the same circumstances as those used for the synthesis of pure MOFs; however, the Fe₃O₄ nanoparticles are widely disseminated on the surface of the MOFs, resulting in improved magnetic characteristics. Because of the magnetic properties of the

particles, it has been shown that the Fe_3O_4 nanoparticles tend to cluster together on the surface of the MOFs.

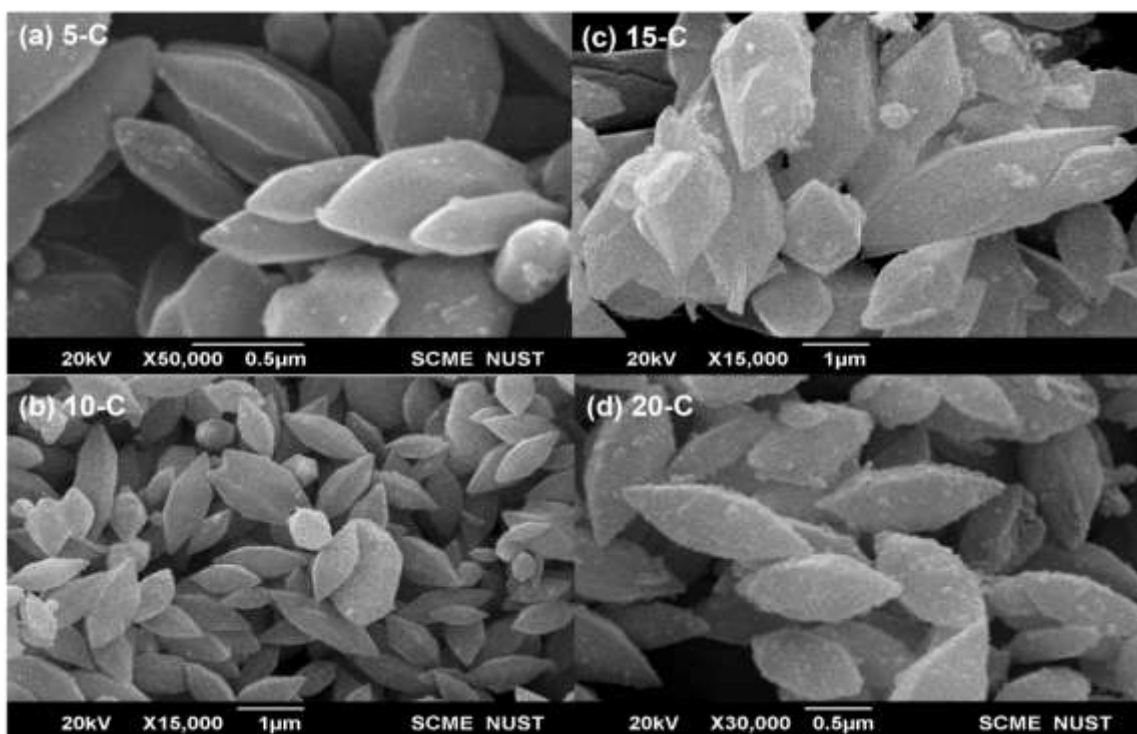


Figure 15: SEM images of different composites (a) 5-C, (b) 10-C, (c) 15-C, (d) 20-C

5.4 Drug Loading of Nanoparticles:

5.4.1 Standard Curve of Ciprofloxacin:

To determine the ciprofloxacin standard curve, various dilutions were prepared, and a graph was drawn between absorbance and concentration. 0.2 mg/ml, 0.3 mg/ml, 0.5 mg/ml, and 0.9 mg/ml of ciprofloxacin solution were prepared to calculate the standard curve. At 323 nanometers, absorbance was measured to determine the quantity of substance based on absorbance at various dilutions.

Table 1: Absorbance values of ciprofloxacin at various concentrations

Concentration mg/ml	Absorbance		Mean
	1	2	
0.2	0.3937	0.3462	0.342
0.3	0.3426	0.3454	0.343
0.5	0.3482	0.3459	0.345
0.9	0.3521	0.3475	0.349

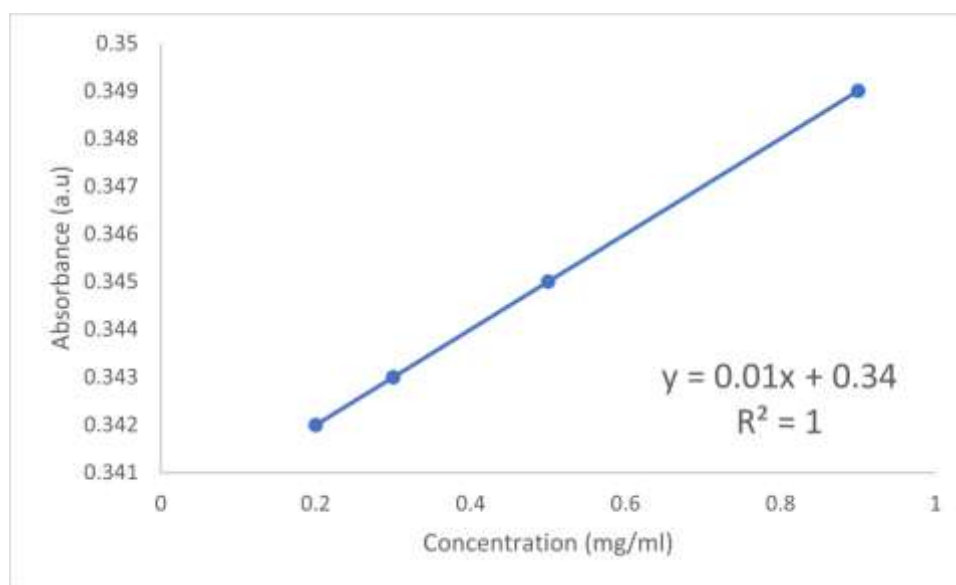


Figure 16: Standard curve for ciprofloxacin

5.4.2 Drug Loading on Nanoparticles:

$$\text{Encapsulation efficiency(\%)} = \frac{\text{Initial drug weight} - \text{Free drug weight in supernatant}}{\text{Initial drug weight}}$$

The quantification of the remaining DOX in The final product was obtained through the quantification of absorbance at 323 nanometers. This value was afterwards compared to the ciprofloxacin standard curve in order to ascertain the drug quantity in relation to the absorbance value.

Table 2: Encapsulation efficiency of composites.

Sample	Absorbance	Relative drug weight (mg/ml)	Initial drug weight (mg/ml)	Encapsulation efficiency (%)
5-C	0.382	4.28	20	78.6
10-C	0.387	4.71	20	75.95
15-C	0.37	3.03	20	84.85
20-C	0.365	2.51	20	87.45

The remaining drug concentration, detected at 323 nanometers by uv-vis spectrophotometer, was measured using ciprofloxacin's standard method. Using absorbance values, the relative drug weight was determined. Composite 5-C (MOF loaded with 5% nanoparticles) exhibited an encapsulation efficiency of 78.6%, whereas encapsulation efficiency increases as the loading amount increases from 5 to 20%, composite loaded with 20% nanoparticles is estimated to have the maximum encapsulation efficiency among all samples.

5.4.3 Drug Release Studies:

In vitro drug release experiments of the produced composites were carried out for a total of 24 hours in a phosphate buffer with a pH of 7.4 and a temperature of 37 degrees Celsius. The total amount of medication that was released throughout the preparation process was tracked and can be found in Table. Figure displays the formulation's graphical representation of the time versus percent cumulative drug release (CDR) plot. This plot provides information about the release of the medication over time. Over the course of time, the value of absorbance goes from 0.82 to 2.3 in case of 5-C, similar behavior with slight changes has been shown by other composites. The investigation that was done on the drug release from the manufactured composites showed that there was a sustained release of drug for around 50% of the loaded drug within 12 hours. Within

twenty-four hours, almost 60 percent of the medicine had been distributed. The highest percentage of drug release is shown by 20-C that means MOF with large amount of nanoparticles can load higher amount of drug and can release it on a relatively fast manner. The pattern of drug release reveals that the medicine is released in a steady manner over the course of 12 hours.

Table 3: percentage drug release data of composites.

Time (hrs.)	5-C		10-C		15-C		20-C	
	Absorbance	% Release	Absorbance	% Release	Absorbance	% Release	Absorbance	% Release
0.5	0.82	12.7	0.88	15.1	0.59	6.5	0.65	8.09
1	0.96	17.22	0.93	16.3	0.82	12.53	0.76	10.97
2	1.24	25.27	1.1	21	1.16	21.42	0.92	15.15
4	1.56	33.8	1.3	26	1.62	33.69	1.42	28.21
6	1.79	39	1.86	42	1.78	37.61	1.66	34.48
24	2.3	54	2.52	56.9	2.2	48.58	2.6	59.03

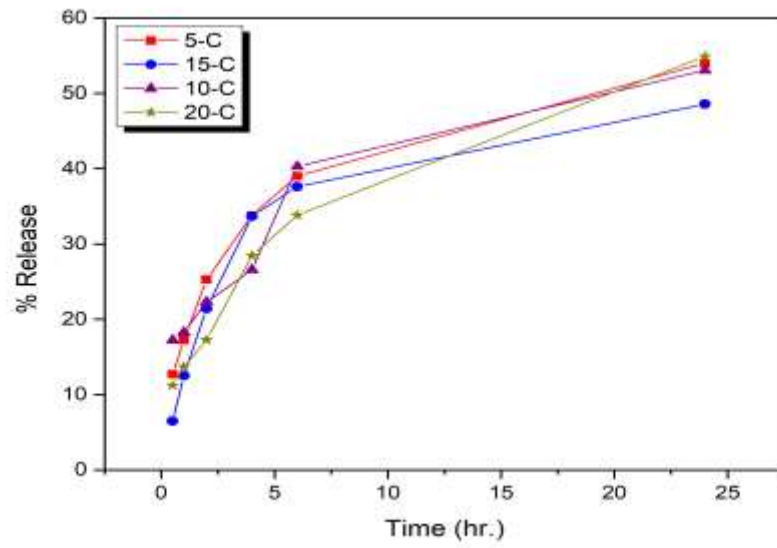


Figure 17: percentage drug release of all composites

Conclusion

In conclusion, we were able to establish a methodology for the synthesis of amine-functionalized magnetic MOFs for drug delivery application. Various quantities of magnetic nanoparticles were applied onto the surface of a Metal-Organic Framework (MOF) in order to examine the profile of drug release. The studies made using the FESEM technique show that magnetic nanoparticles are deposited on the MOFs' surface. Based on the findings of the Fourier Transform Infrared (FTIR) analysis, Ciprofloxacin drug is effectively loaded on the surface of magnetic NH₂-MIL- 88B/ Fe₃O₄. MOF with highest amount of loaded magnetic nanoparticles show highest ability to load the drug which is 87%. 24 hours drug release study is done to check the ability of different composites. MOF having 20% magnetic nanoparticles shows maximum release of drug within 24 hours.it can be concluded that amine-functionalized magnetic MOFs can be a good carrier for drug delivery.

Reference:

- [1] Samrot, A.V., et al., A review on synthesis, characterization and potential biological applications of superparamagnetic iron oxide nanoparticles. (2021). **4**: p. 100042.
- [2] Rai-Choudhury, P., Handbook of microlithography, micromachining, and microfabrication: microlithography. Vol. 39. (1997): SPIE press.
- [3] Mattox, D.M.J.S. and C. technology, Ion plating—past, present and future. (2000). **133**: p. 517-521.
- [4] Kim, D., et al., Synthesis and characterization of surfactant-coated superparamagnetic monodispersed iron oxide nanoparticles. (2001). **225**(1-2): p. 30-36.
- [5] Davis, S.J.T.i.b., Biomedical applications of nanotechnology—implications for drug targeting and gene therapy. (1997). **15**(6): p. 217-224.
- [6] Alavijeh, A.A., et al., The potential of magnetic nanoparticles for diagnosis and treatment of cancer based on body magnetic field and organ-on-the-chip. (2019). **9**(3): p. 360.
- [7] S Wadajkar, A., et al., Design and application of magnetic-based theranostic nanoparticle systems. (2013). **6**(1): p. 47-57.
- [8] Lee, J.-H., et al., Magnetic nanoparticles for multi-imaging and drug delivery. (2013). **35**: p. 274-284.
- [9] Srivastava, A., et al., Polymers in drug delivery. (2015). **4**(1): p. 69-84.
- [10] Vroman, I. and L.J.M. Tighzert, Biodegradable polymers. (2009). **2**(2): p. 307-344.
- [11] Middleton, J.C. and A.J.J.B. Tipton, Synthetic biodegradable polymers as orthopedic devices. (2000). **21**(23): p. 2335-2346.
- [12] Kim, S.-N., et al., Metal-organic frameworks, NH₂-MIL-88 (Fe), as carriers for ophthalmic delivery of brimonidine. (2018). **79**: p. 344-353.
- [13] Arruebo, M., et al., Magnetic nanoparticles for drug delivery. (2007). **2**(3): p. 22-32.

- [14] Hu, F., K. Neoh, and E.J.B. Kang, Synthesis and in vitro anti-cancer evaluation of tamoxifen-loaded magnetite/PLLA composite nanoparticles. (2006). **27**(33): p. 5725-5733.
- [15] Lombardo, D., M.A. Kiselev, and M.T.J.J.o.n. Caccamo, Smart nanoparticles for drug delivery application: development of versatile nanocarrier platforms in biotechnology and nanomedicine. (2019). **2019**.
- [16] Mornet, S., et al., Magnetic nanoparticle design for medical diagnosis and therapy. (2004). **14**(14): p. 2161-2175.
- [17] Liu, Y., et al., 基于磁性质的药物递送系统. (2017). **60**: p. 471-486.
- [18] Medeiros, S., et al., Stimuli-responsive magnetic particles for biomedical applications. (2011). **403**(1-2): p. 139-161.
- [19] Panyam, J. and V.J.A.d.d.r. Labhasetwar, Biodegradable nanoparticles for drug and gene delivery to cells and tissue. (2003). **55**(3): p. 329-347.
- [20] Kumar, C.S. and F.J.A.d.d.r. Mohammad, Magnetic nanomaterials for hyperthermia-based therapy and controlled drug delivery. (2011). **63**(9): p. 789-808.
- [21] Gnanaprakash, G., et al., Effect of initial pH and temperature of iron salt solutions on formation of magnetite nanoparticles. (2007). **103**(1): p. 168-175.
- [22] Wu, W., et al., Recent progress on magnetic iron oxide nanoparticles: synthesis, surface functional strategies and biomedical applications. (2015). **16**(2): p. 023501.
- [23] Li, J., et al., Analysis of the factors affecting the magnetic characteristics of nano-Fe₃O₄ particles. (2011). **56**: p. 803-810.
- [24] Roth, H.-C., et al., Influencing factors in the CO-precipitation process of superparamagnetic iron oxide nano particles: A model based study. (2015). **377**: p. 81-89.
- [25] Mascolo, M.C., Y. Pei, and T.A.J.M. Ring, Room temperature co-precipitation synthesis of magnetite nanoparticles in a large pH window with different bases. (2013). **6**(12): p. 5549-5567.

- [26] Mazrouaa, A.M., M.G. Mohamed, and M.J.E.J.o.P. Fekry, Physical and magnetic properties of iron oxide nanoparticles with a different molar ratio of ferrous and ferric. (2019). **28**(2): p. 165-171.
- [27] Huber, D.L.J.S., Synthesis, properties, and applications of iron nanoparticles. (2005). **1**(5): p. 482-501.
- (28) Ocsoy, I., et al., Biomolecules incorporated metallic nanoparticles synthesis and their biomedical applications. (2018). **212**: p. 45-50.
- [29] Khan, I., K. Saeed, and I.J.A.j.o.c. Khan, Nanoparticles: Properties, applications and toxicities. (2019). **12**(7): p. 908-931.
- [30] Tancredi, P., et al., Exploring the synthesis conditions to control the morphology of gold-iron oxide heterostructures. (2019). **12**: p. 1781-1788.
- [31] Liu, H.-L., et al., One-pot polyol synthesis of monosize PVP-coated sub-5 nm Fe_3O_4 nanoparticles for biomedical applications. (2007). **310**(2): p. e815-e817.
- [32] Wan, J., et al., Monodisperse water-soluble magnetite nanoparticles prepared by polyol process for high-performance magnetic resonance imaging. (2007)(47): p. 5004-5006.
- [33] Yavuz, C.T., et al., Low-field magnetic separation of monodisperse Fe_3O_4 nanocrystals. (2006). **314**(5801): p. 964-967.
- [34] Papaefthymiou, G., et al. Hybrid magnetic nanoparticles derived from wüstite disproportionation reactions at the nanoscale. in ICAME 2005: Proceedings of the 28th International Conference on the Applications of the Mössbauer Effect (ICAME 2005) held in Montpellier, France, 4–9 September 2005, Volume I (Part I–II/V). (2007). Springer.
- [35] Bakrania, S., et al., An investigation of the thermal decomposition of gold acetate. (2009). **95**(1): p. 117-122.
- [36] Tago, T., et al., Novel synthesis of silica- coated ferrite nanoparticles prepared using water- in- oil microemulsion. (2002). **85**(9): p. 2188-2194.
- [37] Poddar, P., et al., Magnetic properties of conducting polymer doped with manganese–zinc ferrite nanoparticles. (2004). **15**(10): p. S570.
- [38] Das, N., et al., Nanosized bismuth ferrite powder prepared through sonochemical and microemulsion techniques. (2007). **61**(10): p. 2100-2104.

- [39] Tadić, M., et al., Synthesis, morphology, microstructure and magnetic properties of hematite submicron particles. (2011). **509**(28): p. 7639-7644.
- [40] Bhaumik, A., S. Samanta, and N.J.P. Mal, Iron oxide nanoparticles stabilized inside highly ordered mesoporous silica. (2005). **65**: p. 855-862.
- [41] Suh, W.H. and K.S.J.J.o.t.A.C.S. Suslick, Magnetic and porous nanospheres from ultrasonic spray pyrolysis. (2005). **127**(34): p. 12007-12010.
- [42] Itoh, H., T.J.J.o.c. Sugimoto, and i. science, Systematic control of size, shape, structure, and magnetic properties of uniform magnetite and maghemite particles. (2003). **265**(2): p. 283-295.
- [43] Figueroa, S., et al., Hyperfine study on sol-gel derived-hematite doped zirconia. (2005). **17**(13): p. 3486-3491.
- [44] Mourdikoudis, S., R.M. Pallares, and N.T.J.N. Thanh, Characterization techniques for nanoparticles: comparison and complementarity upon studying nanoparticle properties. (2018). **10**(27): p. 12871-12934.
- [45] Yang, H., et al., Metal–organic framework coated titanium dioxide nanorod array p–n heterojunction photoanode for solar water-splitting. (2019). **12**: p. 643-650.
- [46] Xing, X.-S., et al., High proton conduction in an excellent water-stable gadolinium metal–organic framework. (2019). **55**(9): p. 1241-1244.
- [47] Hu, C., et al., Toughening mechanisms of epoxy resin using aminated metal-organic framework as additive. (2019). **240**: p. 113-116.
- [48] Howlader, P. and P.S.J.I.J.o.C. Mukherjee, Solvent directed synthesis of molecular cage and metal organic framework of copper (II) paddlewheel cluster. (2019). **59**(3-4): p. 292-298.
- [49] Kampouri, S., et al., Concurrent photocatalytic hydrogen generation and dye degradation using MIL- 125- NH₂ under visible light irradiation. (2018). **28**(52): p. 1806368.
- [50] Yang, Q., et al., Metal–organic- framework- derived hollow N- doped porous carbon with ultrahigh concentrations of single Zn atoms for efficient carbon dioxide conversion. (2019). **131**(11): p. 3549-3553.
- [51] Yang, F., et al., A GO-induced assembly strategy to repair MOF nanosheet-based membrane for efficient H₂/CO₂ separation. (2018). **11**(1): p. 990-997.

- [52] Rajak, R., M. Saraf, and S.M.J.J.o.m.c.A. Mobin, Robust heterostructures of a bimetallic sodium–zinc metal–organic framework and reduced graphene oxide for high-performance supercapacitors. (2019). **7**(4): p. 1725-1736.
- [53] Huan, W., et al., Facile fabrication of magnetic metal–organic framework nanofibers for specific capture of phosphorylated peptides. (2018). **7**(2): p. 2245-2254.
- [54] Mahmoodi, N.M., M. Taghizadeh, and A.J.J.o.M.L. Taghizadeh, Activated carbon/metal-organic framework composite as a bio-based novel green adsorbent: Preparation and mathematical pollutant removal modeling. (2019). **277**: p. 310-322.
- [55] Wang, C.-Y., et al., A mixed valence Tb (III)/Tb (IV) metal–organic framework: Crystal structure, luminescence property and selective detection of naproxen. (2019). **159**: p. 298-307.
- [56] Pang, J., et al., Exploring the sandwich antibacterial membranes based on UiO-66/graphene oxide for forward osmosis performance. (2019). **144**: p. 321-332.
- [57] Zhang, L., et al., A non-enzymatic voltammetric xanthine sensor based on the use of platinum nanoparticles loaded with a metal-organic framework of type MIL-101 (Cr). Application to simultaneous detection of dopamine, uric acid, xanthine and hypoxanthine. (2019). **186**: p. 1-10.
- [58] Mohaghegh, N., M. Faraji, and A.J.A.P.A. Abedini, Highly efficient multifunctional Ag/TiO₂ nanotubes/Ti plate coated with MIL-88B (Fe) as a photocatalyst, adsorbent, and disinfectant in water treatment. (2019). **125**: p. 1-10.
- [59] Kim, M.-K., et al., Degradation of chemical warfare agents over cotton fabric functionalized with UiO-66-NH₂. (2018). **8**(72): p. 41633-41638.
- [60] Henrique, A., et al., Separation of hexane isomers in ZIF-8 by fixed bed adsorption. (2018). **58**(1): p. 378-394.
- [61] Yaghi, O.M., et al., Reticular synthesis and the design of new materials. (2003). **423**(6941): p. 705-714.

- [62] Eddaoudi, M., et al., Systematic design of pore size and functionality in isorecticular MOFs and their application in methane storage. (2002). **295**(5554): p. 469-472.
- [63] Yutkin, M., et al., Porous homo-and heterochiral cobalt (II) aspartates with high thermal stability of the metal-organic framework. (2010). **59**: p. 733-740.
- [64] Zavakhina, M., et al., Synthesis and structure of homochiral polymeric praseodymium tartrate. (2011). **60**: p. 2425-2428.
- [65] Zavakhina, M.S., et al., Homochiral Cu (II) and Ni (II) malates with tunable structural features. (2014). **210**(1): p. 125-129.
- [66] Hu, J.-S., et al., A new 2D→ 3D polythreaded framework constructed on an N-centered tripodal linker and copper (I). (2014). **24**(5): p. 290-292.
- [67] Hu, J.-S., et al., Construction of an unusual 3D framework based on V-shaped imidazolyl and oxalate ligands. (2013). **4**(23): p. 231-232.
- [68] Kampan, N.C., et al., Paclitaxel and its evolving role in the management of ovarian cancer. (2015). **2015**.
- [69] Quan, Q., et al., HSA coated iron oxide nanoparticles as drug delivery vehicles for cancer therapy. (2011). **8**(5): p. 1669-1676.
- [70] Dasari, S. and P.B.J.E.j.o.p. Tchounwou, Cisplatin in cancer therapy: molecular mechanisms of action. (2014). **740**: p. 364-378.
- [71] Chen, D., et al., Bortezomib as the first proteasome inhibitor anticancer drug: current status and future perspectives. (2011). **11**(3): p. 239-253.
- [72] Thorn, C.F., et al., Doxorubicin pathways: pharmacodynamics and adverse effects. (2011). **21**(7): p. 440.
- [73] Gao, X., et al., Controllable synthesis of a smart multifunctional nanoscale metal-organic framework for magnetic resonance/optical imaging and targeted drug delivery. (2017). **9**(4): p. 3455-3462.
- [74] Bhattacharjee, A., M.K. Purkait, and S.J.D.T. Gumma, Loading and release of doxorubicin hydrochloride from iron (III) trimesate MOF and zinc oxide nanoparticle composites. (2020). **49**(25): p. 8755-8763.

- [75] Samui, A., et al., Fabrication of a magnetic nanoparticle embedded NH₂-MIL-88B MOF hybrid for highly efficient covalent immobilization of lipase. (2016). **6**(71): p. 66385-66393.
- [76] Nasrabadi, M., M.A. Ghasemzadeh, and M.R.Z.J.N.J.o.C. Monfared, The preparation and characterization of UiO-66 metal–organic frameworks for the delivery of the drug ciprofloxacin and an evaluation of their antibacterial activities. (2019). **43**(40): p. 16033-16040.
- [77] Mohebi Forouzan, M., et al., Preparation and characterization of a novel Fe₃O₄@PAA@ MIL-100 (Cr) metal-organic framework for the drug delivery of ciprofloxacin and investigation of its antibacterial activities. (2022). **52**(9): p. 1318-1324.
- [78] Silva, V., P. Andrade, and M.J.J.M.M.M. Silva, A. Bustamante D., L. De Los Santos Valladares and J. Albino Aguiar. (2013). **343**: p. 138-143.
- [79] Tai, M.F., C.W. Lai, and S.B.J.J.o.N. Abdul Hamid, Facile synthesis polyethylene glycol coated magnetite nanoparticles for high colloidal stability. (2016). **2016**.
- [80] Wang, Y., et al., Synthesis of Fe₃O₄ magnetic fluid used for magnetic resonance imaging and hyperthermia. (2011). **323**(23): p. 2953-2959.
- [81] Pham, M.-H., et al., Novel route to size-controlled Fe–MIL-88B–NH₂ metal–organic framework nanocrystals.(2011). **27**(24): p. 15261-15267.
- [82] Khizar, S., et al., Encapsulation of doxorubicin in magnetic- polymer hybrid colloidal particles of Eudragit E100 and their hyperthermia and drug release studies. (2020). **31**(8): p. 1732-1743.